CD169-mediated restrictive SARS-CoV-2 infection of macrophages induces pro-inflammatory responses

Running title: Innate immune sensing of SARS-CoV-2 in macrophages

Sallieu Jalloh[1, #], Judith Olejnik[1,2, #], Jacob Berrigan[1], Annuurun Nisa[3], Ellen L Suder[1,2], Hisashi Akiyama[1], Maohua Lei[1], Sanjay Tyagi[3], Yuri Bushkin[3], Elke Mühlberger[1,2$], Suryaram Gummuluru[1$*]

[1]Department of Microbiology, Boston University School of Medicine, Boston, MA, USA; [2]National Emerging Infectious Diseases Laboratories, Boston University, Boston, MA, USA; [3]Public Health Research Institute, New Jersey Medical School, Rutgers University, Newark, NJ, USA

# these authors contributed equally

$ these authors contributed equally

*Lead contact

Suryaram Gummuluru, Ph.D.
Department of Microbiology
Boston University School of Medicine
650 Albany St., X343C
Boston, MA 02118
Ph: (617) 358-1774
Fax: (617) 638-4286
Email: rgummulu@bu.edu

Abstract

Exacerbated and persistent innate immune response marked by pro-inflammatory cytokine expression is thought to be a major driver of chronic COVID-19 pathology. Although macrophages are not the primary target cells of SARS-CoV-2 infection in humans, viral RNA and antigens in activated monocytes and macrophages have been detected in post-mortem samples, and dysfunctional monocytes and macrophages have been hypothesized to contribute to a protracted hyper-inflammatory state in COVID-19 patients. In this study, we demonstrate that CD169, a myeloid cell specific I-type lectin, facilitated ACE2-independent SARS-CoV-2 fusion and entry in macrophages. CD169-mediated SARS-CoV-2 entry in macrophages resulted in expression of viral genomic and sub-genomic (sg) RNAs with minimal viral protein expression and no infectious viral particle release, suggesting a post-entry restriction of the SARS-CoV-2 replication cycle. Intriguingly this post-entry replication block was alleviated by exogenous ACE2 expression in macrophages. Restricted expression of viral gRNA and sgRNA in CD169^{+} macrophages elicited a pro-inflammatory cytokine expression (TNFα, IL-6 and IL-1β) in a RIG-I, MDA-5 and MAVS-dependent manner, which was suppressed by remdesivir pre-treatment. These findings suggest that *de novo* expression of SARS-CoV-2 RNA in macrophages contributes to the pro-inflammatory cytokine signature and that blocking CD169-mediated ACE2 independent infection and subsequent activation of macrophages by viral RNA might alleviate COVID-19-associated hyperinflammatory response.

Author Summary

Over-exuberant production of pro-inflammatory cytokine expression by macrophages has been hypothesized to contribute to severity of COVID-19 disease. Molecular mechanisms that contribute to macrophage-intrinsic immune activation during SARS-CoV-2 infection are not fully understood. Here we show that CD169, a macrophage-specific sialic-acid binding lectin, facilitates abortive SARS-CoV-2 infection of macrophages that results in innate immune sensing of viral replication intermediates and production of proinflammatory responses. We identify an ACE2-independent, CD169-mediated endosomal viral entry mechanism that results in cytoplasmic delivery of viral capsids and initiation of virus replication, but absence of infectious viral production. Restricted viral replication in CD169^{+} macrophages and detection of viral genomic and sub-genomic RNAs by cytoplasmic RIG-I-like receptor family members, RIG-I and MDA5, and initiation of downstream signaling via the adaptor protein MAVS, was required for innate immune activation. These studies uncover mechanisms important for initiation of innate immune sensing of SARS-CoV-2 infection in macrophages, persistent activation of which might contribute to severe COVID-19 pathophysiology.

65 **Introduction**

66 Severe acute respiratory syndrome coronavirus 2 (SARS-CoV-2) is the causative agent
67 of the COVID-19 pandemic, which has claimed nearly 6 million deaths worldwide
68 (https://coronavirus.jhu.edu/). Severe COVID-19 cases have been associated with
69 aberrant bronchioalveolar immune cell activation and persistently high levels of
70 proinflammatory cytokines, including IL-6, TNFα, and IL-1β (1, 2). This protracted immune
71 hyperactivation state marked by uncontrolled proinflammatory cytokine expression (3-6)
72 is a potential driver of acute respiratory distress syndrome (ARDS) in severe COVID-19.
73 Transcriptomic analysis of bronchioalveolar lavage fluid (BALF) samples from SARS-
74 CoV-2 infected individuals revealed extensive lung infiltration by inflammatory monocytes
75 and activated tissue-resident and BALF-associated macrophages with robust induction of
76 interferon-stimulated gene (ISG) expression (7), suggestive of a myeloid cell-intrinsic
77 cytokine signature contributing to ARDS and COVID-19 pathologies (8, 9). However,
78 whether SARS-CoV-2 can establish productive infection in monocytes and macrophages
79 has remained contentious (10-15), and importantly, the molecular mechanisms that
80 contribute to myeloid cell-intrinsic hyperinflammatory phenotype have remained unclear
81 (6, 16-19).

82 Studies on post-mortem tissues from patients, who succumbed to COVID-19,
83 showed that a subset of tissue-resident alveolar macrophages are enriched in SARS-
84 CoV-2 RNA (20, 21). Additionally, single-cell RNA-seq analysis revealed the presence of
85 viral mRNAs in inflammatory myeloid cell populations in autopsied lung tissues (22, 23).
86 Recent studies suggest that tissue-resident human macrophages are permissive to
87 SARS-CoV-2 infection in humanized mice models, and that inhibition of viral genome
88 replication or type-I interferon (IFN) signaling significantly attenuates chronic macrophage

89 hyperactivation and disease progression (24). However, whether the presence of viral
90 RNA in macrophages reflects phagocytosis of infected bystander cells or active virus
91 replication in tissue-resident macrophages has yet to be defined. In contrast, $CD14^+$
92 peripheral blood monocytes, monocyte-derived dendritic cells (MDDCs), or monocyte-
93 derived macrophages (MDMs) were not-permissive to productive SARS-CoV-2 replication
94 in vitro (10-12, 15). In permissive lung epithelial cells and those expressing the cognate
95 entry receptor, angiotensin-converting enzyme 2 (ACE2), SARS-CoV-2 utilizes its spike
96 (S) glycoprotein to interact with ACE2, which facilitates proteolytic cleavage, plasma or
97 endosomal membrane fusion, and cytosolic import of viral genome (25-27). Depending
98 on cell type, different host proteases such as furin, TMPRSS2, or cathepsins are required
99 for S cleavage and entry of SARS-CoV-2 (26, 28, 29). While circulating monocytes and
100 macrophages are not known to express ACE2 (30), these cells have been shown to
101 express low levels of endogenous surface TMPRSS2 (31), and moderate levels of
102 endosomal cathepsins (32) (33), although the relative expression of these cellular
103 proteases in the context of SARS-CoV-2 infection and inflammation is not well understood.
104 Recent reports have highlighted capture of SARS-CoV-2 virus particles by myeloid
105 cell-specific receptors, such as C-type lectins, in an ACE2-independent manner (16, 17,
106 19, 34, 35) though virus particle fusion or productive viral infection was not observed. We
107 and others have previously shown that CD169/Siglec-1 facilitates viral infections of
108 macrophages or dendritic cell (DC)-mediated trans infection of bystander cells (36-39).
109 CD169 binds to sialylated viral glycoproteins or viral membrane-associated gangliosides,
110 GM1 and GM3 (38-44). SARS-CoV-2 S protein is highly sialylated (45, 46), and a recent
111 report demonstrated that DC-mediated SARS-CoV-2 trans infection of $ACE2^+$ epithelial
112 cells was facilitated by CD169 (19). CD169 is highly expressed by splenic red pulp and

113 perifollicular macrophages, subcapsular sinus macrophages (47) and alveolar
114 macrophages (48, 49). Besides constitutive expression on tissue-resident macrophages,
115 CD169 expression can be upregulated on peripheral blood monocytes under inflammatory
116 conditions, especially in response to type I interferons (IFNs) (50-52). Since type I IFNs
117 are highly upregulated and CD169-expressing myeloid cells are elevated during SARS-
118 CoV-2 infection (53, 54), we reasoned that SARS-CoV-2 S mediated interactions with
119 CD169^{+} macrophages might play a crucial role in driving immunopathology of SARS-CoV-
120 2 infection.

121 In this study, we examined the role of CD169 in facilitating SARS-CoV-2 infection
122 of ACE2-deficient human macrophages and its effect on inducing pro-inflammatory
123 cytokine expression. Using two different human macrophage models, PMA-differentiated
124 THP1 cells (THP1/PMA) and primary monocyte-derived macrophages (MDMs), we show
125 that CD169 binds to SARS-CoV-2 S and mediates SARS-CoV-2 S-dependent viral entry
126 into macrophages, leading to restricted cytosolic expression of viral genomic and sub-
127 genomic (sg) RNA. Surprisingly, induced constitutive expression of ACE2 in macrophages
128 (THP1/PMA and MDMs) restored permissiveness to robust virus replication and
129 production of infectious progeny virions, suggesting that ACE2 expression overcomes a
130 post-entry block to SARS-CoV-2 infection in macrophages. While CD169-mediated,
131 ACE2-independent SARS-CoV-2 entry into macrophages resulted in negligible viral
132 protein expression and absence of infectious virus production, restricted expression of
133 viral negative strand RNA and sgRNAs induced pro-inflammatory cytokine expression via
134 retinoic acid-inducible gene I (RIG-I) and melanoma differentiation-associated gene 5
135 (MDA-5) dependent sensing of viral replication intermediates. Importantly, expression of
136 IL-6, TNFα and IL-1β was enhanced, whereas type I IFN responses were muted,

137 suggesting a novel CD169-mediated, macrophage-intrinsic amplification of pro-
138 inflammatory responses. These findings suggest that induction of pro-inflammatory
139 responses in SARS-CoV-2-exposed macrophages requires initial viral RNA synthesis and
140 that abortively infected macrophages might contribute to the hyperimmune phenotype and
141 pathophysiology of COVID-19.
142
143 **Results**
144 **SARS-CoV-2 Spike protein can mediate ACE2-independent entry into macrophages**
145 To examine the role of macrophages in SARS-CoV-2 infection and COVID-19
146 pathogenesis, we differentiated primary MDMs from multiple donors by culturing $CD14^+$
147 monocytes in the presence of human AB-serum and M-CSF for 6 days (55). Compared
148 to a control HEK293T/ACE2 cell line retrovirally transduced to stably express human
149 ACE2, ACE2 expression in primary human MDMs was under the detection limit (**Fig. 1A**
150 **and B**). However, similar to HEK293T/ACE2 cells (**Fig. 1C**), MDMs from multiple donors
151 were robustly infected with a SARS-CoV-2 S-pseudotyped lentivirus (**Fig. 1D**), suggesting
152 that macrophages can support ACE2-independent S-pseudotyped virus entry.
153 Furthermore, SARS-CoV-2 S-pseudotyped infections in MDMs were blocked by pre-
154 treatment with a cathepsin inhibitor (E64D) but not a TMPRSS2 inhibitor (Camostat) (**Fig.**
155 **1D**), suggesting that SARS-CoV-2 S facilitates endosomal viral entry into ACE2-deficient
156 MDMs. Preferential engagement of endosomal entry mechanism for SARS-CoV-2 S
157 pseudotyped lentiviruses (LVs) in MDMs correlated with lack of active and cleaved form
158 of serine protease TMPRSS2 expression in THP1/PMA and primary macrophages ((56),
159 **Fig. S1A**), and robust cathepsin-L expression in THP1/PMA and MDMs (**Fig. S1B**).
160 Strikingly, pre-treatment with neutralizing antibodies targeting the N-terminal domain

161 (NTD) of SARS-CoV-2 S that do not compete with ACE2 binding by S (57), led to
162 significant reduction in S-pseudotyped lentivirus infection of primary MDMs, suggesting
163 that specific interaction between SARS-CoV-2 S and ACE2-independent entry factors are
164 essential to mediate entry and endosomal fusion in macrophages (**Fig. S2**).
165

166 **CD169 is a SARS-CoV-2 attachment and entry factor in macrophages**

167 Expression of CD169, an ISG, is significantly upregulated in monocytes and alveolar
168 macrophages isolated from COVID-19 patients, and its expression enhancement
169 correlates with COVID-19 disease severity (7, 53). While co-expression of CD169 with
170 ACE2 can enhance ACE2-mediated SARS-CoV-2 S entry in HEK293T cells (16), whether
171 CD169 plays a role in SARS-CoV-2 infection of ACE2-deficient macrophages is unclear.
172 To address this question, THP1 cells stably expressing wildtype (wt) CD169, mutant
173 CD169/R116A which displays an attenuated ability to bind sialylated glycoconjugates (39,
174 58, 59), ACE2, or both wt CD169 and ACE2 (CD169/ACE2) (**Fig. S3A**) were incubated
175 with recombinant SARS-CoV-2 S protein, and relative S binding was determined by flow
176 cytometry. In contrast to parental THP1 monocytes, THP1 cells expressing wt CD169
177 (THP1/CD169) displayed robust S binding comparable to levels observed with
178 THP1/ACE2 cells (**Fig. 2A**). There was a significant reduction in S binding to
179 THP1/CD169-R116A cells, indicating that the sialylated S protein is recognized by CD169
180 (**Fig. 2A**). Co-expression of CD169 and ACE2 in THP1 cells further enhanced S binding
181 compared to cells expressing only ACE2 or CD169, suggestive of cooperative binding of
182 CD169 and ACE2 to SARS-CoV-2 S.

183 We next sought to determine the role of CD169 in mediating SARS-CoV-2 infection
184 of macrophages. PMA-differentiated THP1 macrophages expressing wt or mutant CD169,

185 ACE2, or CD169/ACE2 were infected with SARS-CoV-2 S-pseudotyped lentiviruses.
186 Expression of wt CD169 on THP1/PMA macrophages enhanced S-pseudotyped lentiviral
187 infection by ~30-fold compared to parental THP1/PMA macrophages, similar to the levels
188 of infection observed with $ACE2^+$ THP1/PMA macrophages (**Fig. 2B**). In contrast
189 expression of CD169/R116A did not enhance S-pseudotyped lentiviral infection of
190 THP1/PMA cells, confirming that recognition of sialylated motifs on SARS-CoV-2 S is
191 essential for CD169-mediated infection of macrophages (**Fig. 2B**). Co-expression of wt
192 CD169 and ACE2 further enhanced S-pseudotyped lentiviral infection by greater than 11-
193 fold and 3-fold when compared to cells expressing CD169 or ACE2, respectively (**Fig.**
194 **2B**), confirming that CD169 facilitates S-mediated entry into macrophages in the absence
195 of ACE2 and enhances entry in the presence of ACE2. To confirm the role of CD169 in
196 SARS-CoV-2 S-mediated infection in primary human MDMs, and given the relatively low
197 and variable expression of endogenous CD169 in primary MDMs (**Fig. S3B**), we used
198 lentiviral transduction to overexpress either wt CD169 or ACE2 (**Fig. S3C and D**).
199 Following infection of transduced primary macrophages with S-pseudotyped lentivirus, we
200 observed that CD169 or ACE2 overexpression in MDMs from multiple donors significantly
201 enhanced SARS-CoV-2 S-pseudotyped lentivirus infection compared to control MDMs
202 transduced with empty vector (**Fig. 2C**). Crucially, pre-treatment with anti-CD169 blocking
203 mAb (7D2) prior to infection with S-pseudotyped lentivirus significantly attenuated
204 infection of untransduced primary MDMs when compared to non-specific IgG1
205 pretreatment (**Fig. 2D**). These findings suggest that CD169 facilitates SARS-CoV-2 S-
206 dependent fusion and entry into both THP1/PMA macrophages and primary MDMs in the
207 absence of ACE2.
208

209 **SARS-CoV-2 establishes abortive infection in macrophages lacking ACE2**

210 To investigate whether CD169 expression is sufficient to establish productive SARS-CoV-
211 2 infection and replication in ACE2-deficient macrophages, we infected THP1/PMA and
212 primary MDMs overexpressing CD169, ACE2, or parental cells (lacking both CD169 and
213 ACE2) with replication-competent SARS-CoV-2 (Washington isolate, NR-52281), as
214 previously described (60). To evaluate productive infection, we examined the temporal
215 expression of double-stranded RNA (dsRNA), a viral replication intermediate (61), as well
216 as viral nucleocapsid (N) protein. SARS-CoV-2-infected THP1/PMA macrophages were
217 fixed at various time points post infection and subjected to immunofluorescence analysis
218 using antibodies against dsRNA and SARS-CoV-2 N. In contrast to parental THP1/PMA
219 macrophages that showed background staining of dsRNA and no expression of SARS-
220 CoV-2 N at any time point post infection (**Fig. 3A**), CD169-expressing THP1/PMA cells
221 showed low levels of dsRNA production and small puncta staining of SARS-CoV-2 N that
222 did not significantly increase over the course of infection (**Fig. 3B**). However, both ACE2$^+$
223 (**Fig. 3C**) and CD169/ACE2 double-positive (**Fig. 3D**) THP1/PMA macrophages showed
224 robust dsRNA and SARS-CoV-2 N production starting as early as 2-4 hours post infection
225 (hpi), which significantly increased over the course of infection. There was a clear
226 distinction in the spatial distribution of viral N protein in infected ACE2$^+$ and
227 CD169$^+$/ACE2$^+$ THP1/PMA macrophages over time, as noted by a transition from 6 hpi
228 onward from small cytosolic N protein puncta to homogenous distribution throughout the
229 cytosol (**Fig. 3C** and **D**). Furthermore, there was extensive co-localization between peri-
230 nuclear dsRNA foci and N staining in ACE2$^+$ and CD169$^+$/ACE2$^+$ THP1/PMA
231 macrophages at 6 and 24 hpi. In accordance with our S-pseudotyped lentivirus infection
232 data (**Fig. 2B**), co-expression of CD169 and ACE2 led to an increase in SARS-CoV-2

233 infection compared to ACE2-expressing cells, with higher levels and slightly earlier
234 production of dsRNA and SARS-CoV-2 N (compare **Fig. 3C** and **D**). In contrast, N protein
235 staining was not dispersed in the cytoplasm of CD169^{+} THP1/PMA macrophages and
236 remained as small cytosolic puncta over the course of infection with minimal co-
237 localization with dsRNA staining (**Fig. 3B**). These findings suggest that CD169-mediated
238 SARS-CoV-2 entry in THP1/PMA macrophages results in initiation of viral transcription
239 and moderate viral protein production.

240 Similar to our findings in THP1/PMA macrophages, we observed SARS-CoV-2 N
241 expression in primary MDMs overexpressing ACE2, whereas we were not able to detect
242 N protein in primary untransduced MDMs or those overexpressing CD169 at 24 hpi (**Fig.**
243 **S4**). The lack of detection of either N (**Fig. S4**) or dsRNA (data not shown) in primary
244 MDMs compared to the low level of N and dsRNA expression observed in THP1/CD169
245 macrophages (**Fig. 3B**) could be explained by the inefficient lentivector transduction
246 efficiency and low expression of CD169 in primary MDMs (**Fig. S3B** and **C**) compared to
247 the robust CD169 expression in retrovirally transduced THP1 cells (**Fig. S3A**). We further
248 quantified infectious SARS-CoV-2 particle production from both THP1/PMA macrophages
249 (**Fig. 3E**) and primary MDMs (**Fig. 3F**) by TCID50 assay and detected no infectious virions
250 in culture supernatants from CD169-expressing cells. However, both THP1/PMA and
251 primary MDMs expressing ACE2 showed robust production of infectious SARS-CoV-2
252 particles, with a marked increase in infectious virus production in THP1/PMA cells co-
253 expressing CD169 and ACE2 compared to ACE2 alone (**Fig. 3E**). These results suggest
254 an absence of post-entry restrictions to SARS-CoV-2 replication in macrophages, if virus
255 entry is mediated by ACE2.
256

257 **CD169-mediated SARS-CoV-2 infection of macrophages results in *de novo***
258 **expression of viral mRNAs**

259 To explore the spatial and temporal distribution of SARS-CoV-2 RNA at single cell level,
260 single-molecule RNA FISH (smFISH) analysis (62) was performed in infected THP1/PMA
261 macrophages. Individual fluorescent spots corresponding to viral gRNAs were detected
262 in CD169$^+$, ACE2$^+$ and CD169$^+$/ACE2$^+$ THP1/PMA macrophages, as early as 1 hpi (**Fig.**
263 **S5**). By 6 hpi, we observed diffuse cytosolic staining and perinuclearly localized bright
264 gRNA foci (**Fig. S5**), which further increased in in ACE2$^+$ and CD169$^+$/ACE2$^+$ but not
265 CD169$^+$ THP1/PMA macrophages (**Fig. S5**). In order to distinguish between gRNAs and
266 N gene transcripts, we probed cells at 24 hpi with two probe sets labeled with
267 distinguishable dyes one against SARS-CoV-2 ORF1a and the other against N gene. The
268 former detects only gRNA and the later reports both gRNA and N sub-genomic transcripts
269 **(Fig. 4A)**. The staining, particularly that of N gene, showed diffused cytoplasmic
270 distribution, only in ACE2$^+$ and CD169$^+$/ACE2$^+$ THP1/PMA macrophages, especially in
271 the advanced stages of infection.

272 Dispersion of N transcripts (gRNA and sgRNA) in the cytosol of ACE2$^+$ and
273 CD169$^+$/ACE2$^+$ THP1/PMA macrophages mirrors the temporal localization phenotype of
274 viral N protein (**Fig. 3C** and **D**), and might be indicative of formation of N positive viral
275 replication compartments (63). While a majority of virus-exposed CD169$^+$ THP1/MA
276 macrophages expressed fluorescent puncta (gRNA) at 24 hpi (indicated by the white
277 arrowheads showing both ORF1a and N expression**, Fig. 4A and B**), transition to bright
278 gRNA foci or cytosolic expansion was not observed, suggesting that CD169 expression
279 in THP1/PMA cells increased uptake of virus, but without ACE2, failed to establish viral
280 replication foci. It should be noted that the formation of distinct fluorescent puncta in

281 CD169^{+} THP1/PMA macrophages at 24 hpi is suggestive of *de novo* RNA synthesis and
282 not virus inoculum, since these puncta were not detected at 1 hpi (**Fig. S5**). While viral
283 RNAs in the CD169-expressing cells are localized in few distinct granulated puncta,
284 ACE2-expressing cells exhibited inclusion-like structures, suggesting that differential
285 engagement of viral entry receptors (such as CD169 and ACE2) leads to altered fate of
286 the incoming viral genome and subsequent steps in the viral replication cycle.

287 To further investigate the step at which SARS-CoV-2 replication is restricted in
288 macrophages, THP1/PMA macrophages or those expressing either CD169, ACE2, or
289 both CD169 and ACE2 were infected with SARS-CoV-2 and cells lysed and harvested at
290 2, 4, 6, and 24 hpi to quantify the level of total SARS-CoV-2 N transcripts, +gRNA and
291 sgRNA, as well as negative sense antigenomic RNA, by RT-qPCR. We detected
292 increasing levels of total SARS-CoV-2 N transcripts at early time points (2-6 hpi) in
293 THP1/PMA macrophages expressing CD169, ACE2, or both CD169 and ACE2, whereas
294 parental THP1/PMA macrophages showed no significant increase in viral N RNA levels
295 compared to mock infection controls (**Fig. 4C**). Furthermore, there were no significant
296 differences in gRNA levels at early times post infection (up to 6 hpi) between CD169^{+},
297 ACE2^{+} or CD169^{+}/ACE2^{+} THP1/PMA macrophages suggesting an absence of cell-
298 intrinsic restrictions to early steps of SARS-CoV-2 replication, such as attachment and
299 fusion, in CD169+ THP1/PMA macrophages. Interestingly, SARS-CoV-2 N transcripts
300 peaked at 6 hpi in CD169+ THP1/PMA cells, followed by a progressive decline at 24 hpi
301 (**Fig. 4C**). In contrast, there was a temporal increase in SARS-CoV-2 N transcripts in cells
302 expressing ACE2, with markedly higher expression at 24 hpi compared to CD169-
303 expressing cells. In concordance with SARS-CoV-2 N protein expression (**Fig. 3D**),

304 THP1/PMA cells expressing both CD169 and ACE2 expressed the highest levels of
305 SARS-CoV-2 N transcripts at 24 hpi compared to those expressing ACE2 or CD169 alone.
306 After virus entry and capsid uncoating, the next steps in the SARS-CoV-2
307 replication cycle are translation of the viral gRNA followed by the formation of viral
308 replication-transcription complexes, which enables synthesis of the negative sense
309 antigenomic RNA (64). Negative sense antigenomic RNAs are present at significantly
310 lower levels than +gRNA and sgRNA, and are templates for synthesis of additional
311 positive sense gRNA and sgRNAs (64). We employed strand-specific RT-qPCR analysis
312 to detect negative sense viral RNA (ORF1b) and confirmed viral replication (at 2 hpi) in
313 CD169^{+} THP1/PMA cells, compared to complete absence of negative sense viral RNAs
314 in parental THP1/PMA macrophages (**Fig. 4D**). Interestingly, negative sense RNA
315 expression in CD169^{+} THP1/PMA macrophages plateaued at 6 hpi, suggesting that
316 CD169-mediated SARS-CoV-2 entry promotes initial steps of viral replication. In contrast,
317 there was a progressive increase in negative sense RNA levels in ACE2^{+} THP1/PMA
318 macrophages particularly at 24 hpi, and a further enhancement was observed upon co-
319 expression of CD169 and ACE2 in THP1/PMA macrophages at later times post infection
320 (**Fig. 4D**).
321 To confirm that temporal increases in viral transcripts in CD169^{+} or ACE2^{+}
322 THP1/PMA macrophages were generated from ongoing virus transcription, THP1/PMA
323 cells (±CD169 ±ACE2) were pre-treated with remdesivir (RDV), a known inhibitor of
324 SARS-CoV-2 RNA synthesis, prior to infection with SARS-CoV-2 (24, 63). RT-qPCR
325 analysis of both gRNA (N transcripts) (**Fig. 4E**) and sgRNA (E transcripts) (**Fig. 4F**)
326 transcripts harvested at 24 hpi revealed that RDV pre-treatment completely blocked the
327 increase in viral RNA expression in THP1/PMA macrophages expressing CD169, ACE2,

328 or both CD169 and ACE2, to levels observed in parental THP1/PMA macrophages.
329 Furthermore, levels of viral gRNA (**Fig. 4G**) and sgRNA (**Fig. 4H**) in SARS-CoV-2 infected
330 untransduced MDMs progressively increased over time, and these increases in viral
331 gRNA and sgRNAs were also suppressed upon RDV pre-treatment. Notably, primary
332 MDMs harbored higher levels of viral transcripts compared to parental THP1/PMA
333 macrophages at all times post infection (**Fig. 4E-H**), suggesting that endogenous CD169
334 expression was sufficient to facilitate entry and initiation of virus replication in primary
335 MDMs. The marked lower levels of viral transcripts in primary MDMs (**Fig. 4G** and **H**)
336 compared to CD169$^+$ THP1/PMA macrophages (**Fig. 4E** and **F**) might be correlated to the
337 lower CD169 expression in primary MDMs compared to CD169$^+$ THP1/PMA
338 macrophages cells which were selected for high CD169 expression (**Fig. S3A**). Taken
339 together, these results suggest that CD169-mediated viral entry enables initiation of viral
340 RNA replication and transcription in ACE2-deficient CD169$^+$ macrophages even in the
341 absence of establishment of robust viral RNA replication foci in macrophages, and that
342 SARS-CoV-2 infection of macrophages is restricted at a post-entry step of virus replication.
343

344 **Low level expression of SARS-CoV-2 genomic and sub-genomic RNAs is sufficient**
345 **to induce pro-inflammatory cytokines in non-productively infected macrophages**

346 Since CD169 expression in macrophages was sufficient to permit SARS-CoV-2 entry and
347 initiate restricted viral RNA expression, we investigated whether *de novo* viral RNA
348 synthesis in the absence of productive virus replication can trigger innate immune
349 responses. SARS-CoV-2 infected THP1/PMA cells (±CD169 ±ACE2) were lysed at 24
350 hpi, and total RNA was analyzed by RT-qPCR for inflammatory cytokine expression (**Fig.**
351 **5**). We observed significant induction of expression of IL-6, TNFα, IL-1β, and IL-18 mRNA

352 in non-productively infected CD169$^+$ THP1/PMA macrophages compared to the parental
353 THP1/PMA cells (**Fig. 5A**). IL-6 and TNFα mRNA expression in SARS-CoV-2 infected
354 THP1/CD169 cells was similar to the levels observed in productively infected THP1/ACE2,
355 but lower than that observed in THP1/CD169/ACE2 cells. Intriguingly, induction of pro-
356 inflammatory cytokines, IL-1β and IL-18, was only consistently observed in non-
357 productively infected THP1/CD169 macrophages but not in the productively infected
358 THP1/ACE2 or THP1/CD169/ACE2 macrophages (**Fig. 5A**). A delayed or impaired type I
359 IFN response is thought to be a critical mechanism for COVID-19 pathogenesis, though
360 impaired induction of type I IFN response has mostly been reported in infected lung
361 epithelial cells (65). Interestingly, we observed muted induction of IFNβ, IP-10 and Viperin
362 in SARS-CoV-2 infected CD169$^+$ THP1/PMA macrophages. In contrast, IFNβ, IFNλ1, IP-
363 10 and Viperin mRNA expression was dramatically upregulated upon establishment of
364 productive SARS-CoV-2 infection in THP1/ACE2 and THP1/CD169/ACE2 macrophages
365 (**Fig. 5A**) and correlated with the extent of viral RNA expression and virus replication in
366 these cells (**Fig. 3**).

367 Since previous reports have suggested that macrophage exposure to recombinant
368 S protein may trigger inflammatory cytokine production (17, 66), we infected parental,
369 CD169$^+$, ACE2$^+$, or CD169$^+$/ACE2$^+$ THP1/PMA cells with S-pseudotyped lentivirus but
370 observed no induction of pro-inflammatory cytokines (IL-6, TNFα, IL-1β, and IFNλ1) (**Fig.
371 S6**). To confirm that the induction of pro-inflammatory cytokine and ISG expression was
372 due to viral replication and sensing of viral RNA, we infected THP1/PMA macrophages
373 with SARS-CoV-2 in the presence of RDV. Pre-treatment with RDV which abolished virus
374 replication (**Fig. 4E** and **F**) completely abrogated IL-6, TNFα, IL-1β and IFNλ1 induction
375 in CD169$^+$, ACE2$^+$, and CD169$^+$/ACE2$^+$ THP1/PMA macrophages (**Fig. 5B**), suggesting

376 that *de novo* viral RNA transcription and sensing of virus replication intermediates are
377 required for the induction of pro-inflammatory cytokines and ISGs in macrophages.
378 Temporal analysis of inflammatory cytokine induction revealed that while SARS-CoV-2
379 infection of parental THP1/PMA cells did not result in induction of pro-inflammatory
380 responses (**Fig. 5C**), infection of CD169^{+} THP1/PMA cells led to rapid induction of IL-6,
381 TNFα, IL-1β, and IFNλ1 mRNA expression (**Fig. 5D**). In fact, fold-induction in levels of
382 pro-inflammatory cytokines at early times post infection (4-6 hpi) was similar between
383 CD169^{+} and ACE2^{+} macrophages (**Fig. 5D** and **E**), indicating that early viral RNA
384 production is the key trigger of innate immune activation. Accelerated kinetics and highest
385 magnitude of induced IFNλ1 expression was observed in SARS-CoV-2 infected
386 CD169^{+}/ACE2^{+} THP1/PMA macrophages (**Fig. 5F,** note difference in scale on y axis),
387 which correlated with greater level of negative sense antigenomic RNA (**Fig. 4D**) and
388 highest levels of virus replication in CD169^{+}/ACE2^{+} THP1/PMA macrophages (**Fig. 3E**).
389 To further confirm the findings obtained from CD169^{+} THP1/PMA macrophages,
390 we pre-treated primary MDMs from multiple donors with RDV for 30 minutes prior to
391 infection with SARS-CoV-2. Total RNA was harvested and subsequently analyzed by RT-
392 qPCR to determine fold-induction of IL-6, TNFα, IL-1β, and IFNλ1 mRNA expression at
393 indicated timepoints (**Fig. 5G**). Similar to the observations in CD169^{+} THP1/PMA
394 macrophages (**Fig. 5B**), SARS-CoV-2 infection induced IL-6, TNFα, IL-1β, and IFNλ1
395 mRNA in primary MDMs (**Fig. 5G**), with proinflammatory cytokine induction observed as
396 early as 2 hpi. Furthermore, induction of pro-inflammatory responses in primary MDMs
397 was significantly suppressed by RDV pre-treatment (**Fig. 5G**), confirming that
398 establishment of infection and initiation of viral transcription is required for macrophage-
399 intrinsic innate immune activation. Collectively, these findings suggest that CD169-

400 mediated restricted SARS-CoV-2 infection of macrophages induces robust inflammatory
401 responses.
402
403 **Cytosolic RNA sensing by RIG-I and MDA-5 is required for SARS-CoV-2 induced**
404 **inflammation in macrophages**
405 Since innate immune activation in THP1/CD169 cells and primary MDMs requires the
406 expression of *de novo* viral RNAs (**Fig. 5B** and **G**), we next sought to delineate the nucleic
407 acid sensing mechanism required for the detection of SARS-CoV-2 gRNA and sgRNAs in
408 CD169^{+} THP1/PMA macrophages. Depending on the specific pathogen-derived cytosolic
409 nucleic acids, numerous host sensors can detect and trigger innate immune activation via
410 the MAVS and/or STING pathways (67). Viral RNAs can be sensed by RIG-I-like receptors
411 (RLRs) or endosomal toll-like receptors (TLRs) to activate MAVS or TRIF, respectively,
412 leading to induction of pro-inflammatory cytokines (68). Innate immune sensing of SARS-
413 CoV-2 RNAs by RLRs such as RIG-I and MDA-5, or endosomal TLRs (TLR7/8), has been
414 previously proposed (69, 70). It has also been hypothesized that SARS-CoV-2-induced
415 mitochondrial damage and release of mitochondrial DNA into the cytosol, a cellular stress
416 response, could trigger cGAS/STING sensing pathway in infected cells (71, 72). To
417 investigate which of the nucleic acid sensing pathways are involved in sensing abortive
418 SARS-CoV-2 infection in macrophages, we stably knocked-down expression of either
419 RIG-I, MDA-5, UNC93B1 (a protein required for TLR3/7/9 trafficking to endosomes, (73)),
420 MAVS or STING in CD169^{+} THP1/PMA cells through shRNA-based lentiviral transduction.
421 Upon successful selection of transduced cells targeted for knockdown of individual host
422 proteins, we observed robust decrease in both mRNA (**Fig. 6A**) and protein (**Fig. 6B**)
423 expression. Knock-down of RIG-I, MDA-5, UNC93B1, MAVS or STING in THP1/CD169

424 macrophages did not impact infection efficiency of SARS-CoV-2, as shown by RT-qPCR
425 analysis of viral gRNA and sgRNAs in each cell line (**Fig. 6C** and **D**). While knockdown of
426 UNC93B1 in virus-infected THP1/PMA CD169$^+$ cells had negligible impact on induction of
427 pro-inflammatory cytokines (IL-6, TNFα, IL-1β and IFNλ1) compared to scramble control
428 cells, depletion of either RIG-I or MDA-5 led to dramatic reduction in pro-inflammatory
429 cytokine expression to near background levels, suggesting both cytosolic viral RNA
430 sensors, but not endosomal TLRs, are required for innate immune sensing of SARS-CoV-
431 2 transcripts (**Fig. 6E-H**). Furthermore, knock-down of MAVS but not STING, completely
432 abrogated SARS-CoV-2- induced innate immune activation in THP1/PMA macrophages,
433 further confirming the requirement of cytosolic viral RNA sensing for induction of pro-
434 inflammatory cytokines.
435
436 **MAVS is essential for SARS-CoV-2 RNA-induced innate immune activation in both**
437 **non-productively and productively infected THP1/PMA macrophages**
438 We next sought to determine if MAVS was required for induction for pro-inflammatory
439 responses not only in CD169-mediated abortive infection but also in ACE2-mediated
440 productive infection of macrophages with SARS-CoV-2. Parental THP1 cells or those
441 expressing CD169, ACE2, or both CD169 and ACE2 were transduced with lentivectors
442 expressing scramble shRNAs (control) or MAVS-specific shRNAs, which led to robust
443 knock-down of MAVS protein expression in all cell lines (**Fig. 7A**). While MAVS depletion
444 did not affect subsequent SARS-CoV-2 infection of CD169$^+$, ACE2$^+$ or CD169$^+$/ACE2$^+$
445 THP1/PMA cells, as quantified by total SARS-CoV-2 N gRNA transcripts (**Fig. 7B**),
446 induction of pro-inflammatory cytokines (IL-6, TNFα, IL-1β and IFNλ1) was significantly
447 attenuated in both productively (ACE2$^+$, CD169$^+$/ACE2$^+$) and abortively (CD169$^+$) infected

448 THP1/PMA macrophages upon MAVS knockdown (**Fig. 7C**). These results suggest that
449 MAVS plays a pivotal role in pro-inflammatory cytokine induction in both ACE2-dependent
450 and independent (CD169-mediated) SARS-CoV-2 infection of THP1/PMA macrophages.
451 Taken together, these findings suggest that CD169-dependent establishment of abortive
452 SARS-CoV-2 infection in macrophages triggers RIG-I/MDA-5 mediated sensing of viral
453 gRNA and sgRNAs and MAVS-dependent inflammatory cytokines induction, which might
454 contribute to the dysregulated hyper-immune phenotype of inflammatory macrophages
455 and severity of COVID-19 disease.
456

457 **Discussion**

458 Though monocytes and macrophages have not been directly implicated in productive
459 SARS-CoV-2 infection, several reports have provided evidence of SARS-CoV-2 RNA and
460 antigen in circulating monocytes, macrophages, and tissue-resident alveolar
461 macrophages, although these cells are not known to express ACE2 (**Fig. 1** and (30).
462 Importantly, macrophage-intrinsic inflammatory phenotype in lung BALF samples has
463 been associated with COVID-19 disease severity (7). In this study, we examined the
464 mechanisms by which macrophages potentially contribute to inflammation during SARS-
465 CoV-2 infection, using THP1/PMA and primary human macrophages expressing a
466 myeloid cell-specific receptor, CD169, in the presence or absence of ACE2. We showed
467 that CD169 expression mediated entry and fusion of SARS-CoV-2 S-pseudotyped
468 lentivirus in both CD169^{+} THP1/PMA and primary macrophages. It was recently reported
469 that CD169 expressed on dendritic cells captures SARS-CoV-2 particles via binding to
470 gangliosides exposed on the viral membrane, such as GM1, and mediates trans infection
471 of bystander cells (19). Our results, however, suggest that CD169 can also bind the

472 sialylated SARS-CoV-2 S protein. Other studies, including ours, have also described
473 glycan-dependent interactions of SARS-CoV-2 S protein with C-type lectin receptors (DC-
474 SIGN, LSIGN) and Tweety family member 2 (TTYH2) (17, 19, 74). While ACE2-
475 independent mechanisms of SARS-CoV-2 interactions with myeloid cells can be mediated
476 by diverse virus particle-associated antigens (gangliosides, mannosylated S and
477 sialylated S), our results suggest that CD169-S interaction is sufficient to promote virus
478 entry and fusion in macrophages in an ACE2-independent manner.

479 Pre-treatment with antibodies targeting SARS-CoV-2 S NTD and inhibition of
480 endosomal cathepsins markedly attenuated S-pseudotyped lentiviral infection in CD169^{+}
481 macrophages, suggesting that S interaction with CD169 and virus entry mechanisms are
482 distinct to those targeted by ACE2. This is in agreement with recent data suggesting that
483 binding epitopes for myeloid cell-specific receptors are found outside the ACE2 binding
484 domain in the spike receptor binding domain (RBD) (17). Consequently, the results
485 presented here have implications for antibody treatment in COVID-19 patients, as current
486 therapies are primarily focused on RBD-binding antibodies (57, 75-78). Targeting non-
487 RBD epitopes to disrupt ACE2-independent entry in CD169^{+} myeloid cells could serve as
488 a potential mechanism for preventing myeloid cell-intrinsic immune activation. Indeed,
489 broadly neutralizing nanobodies and potent NTD-targeting neutralizing antibodies from
490 COVID-19 patients that block both ACE2-dependent and ACE2-independent entry were
491 recently described (57, 75-78) and might provide potential benefit in also suppressing
492 macrophage-intrinsic inflammatory signature.

493 Efficiency of CD169-mediated S-pseudotyped infection in macrophages was
494 similar to that mediated by ACE2 (**Fig. 2**). Importantly, CD169-mediated SARS-CoV-2
495 entry was also similarly efficacious to that mediated by ACE2 in THP1/PMA macrophages,

496 as evident by the similar number of viral gRNA copies at 6 hpi (**Fig. 4C**), though viral
497 gRNA and sgRNA expression in THP1/CD169+ macrophages was attenuated at later
498 times post infection (**Fig. 4E** and **F**). SARS-CoV-2 RNA synthesis occurs within ER-
499 derived double-membrane vesicles (DMVs). The establishment of viral replication
500 factories within DMVs in the cytoplasm of infected cells is induced by viral proteins, in
501 concert with cellular factors (64). Previous reports have utilized dsRNA staining to
502 visualize these viral replication organelles (79). While viral dsRNA+ cells were observed
503 in a minor percentage of THP1/CD169^{+} macrophages at 6 hpi (**Fig. 3B**), no further
504 increase was observed. In contrast, majority of the virus-exposed THP1/ACE2 and
505 THP1/CD169/ACE2 macrophages were dsRNA+ by 24 hpi (**Fig. 3C** and **D**). Since this
506 staining strategy requires expression of high levels of viral dsRNA, the paucity of dsRNA
507 positivity in SARS-CoV-2 infected CD169^{+} macrophages might reflect selective
508 impairment of formation of DMVs. However, expression of ACE2 in THP-1/PMA and
509 primary MDMs restored infectious virus particle production, suggesting that macrophages
510 are permissive to SARS-CoV-2 replication when entry is facilitated by ACE2. Considering
511 that both CD169 and ACE2 mediated virus entry resulted in similar levels of SARS-CoV-
512 2 gRNA at 6 h pi but only ACE2-mediated virus entry resulted in productive virus infection,
513 these results implicate a hitherto unappreciated post-entry role for ACE2 in virus life cycle
514 in macrophages. Interestingly, expression of both CD169 and ACE2 in macrophages led
515 to enhanced kinetics and magnitude of infection, reflecting an entry-enhancing effect of
516 CD169 even in the context of ACE2-mediated infection, though the mechanism of
517 enhanced kinetics of SARS-CoV-2 replication in CD169^{+}/ACE2^{+} macrophages remains
518 unclear.

519 Despite lack of productive infection, cytoplasmic viral RNA expression in CD169$^+$
520 macrophages potently induced expression of pro-inflammatory cytokines and chemokines.
521 Thus, CD169-mediated viral entry does not simply enable viral uptake by macrophages
522 but also initiates SARS-CoV-2 replication and triggers inflammatory cytokine expression.
523 Critically, pre-treatment with RDV not only blocked *de novo* viral RNA expression but also
524 significantly reduced pro-inflammatory cytokine expression in non-productively infected
525 CD169$^+$ macrophages (**Fig. 5**), suggesting that neither S protein interaction with cell
526 surface receptors nor TLR-mediated sensing of incoming viral genome in the endosomal
527 lumen is sufficient to trigger robust innate immune activation. Rather newly synthesized
528 viral RNAs (negative sense gRNA, dsRNA, and/or sgRNAs) are the key drivers of innate
529 immune activation in non-productively infected macrophages. While mRNA expression of
530 type I and III IFNs peaked at 24 hpi and correlated with the extent of virus replication
531 (marked by high levels of IFNλ1 mRNA expression at 24 hpi, **Fig. 5A**), pro-inflammatory
532 cytokines, IL-6 and TNFα mRNAs were induced to comparable levels in both productively
533 (ACE2$^+$ and CD169$^+$/ACE2$^+$) and non-productively (CD169$^+$) infected macrophages (**Fig.**
534 **5A**). Interestingly, significant induction of IL-1β and IL-18 was only observed in CD169+
535 THP1/PMA and primary macrophages (**Fig. 5D** and **G**), suggesting that CD169-mediated
536 virus entry and infection establishment uncouples induction of inflammatory responses
537 from robust viral replication. Since transcriptional priming of the inflammasome
538 components, IL-1β and IL-18, was only observed in abortively infected CD169$^+$
539 THP1/PMA macrophages (**Fig. 5A**), SARS-CoV-2 infected and primed macrophages
540 might thus uniquely contribute to the inflammasome activation upon delivery of secondary
541 activation signals and perpetuate the hyper-inflammatory inflammatory phenotype.

542 Previous reports have implicated both RIG-I and MDA-5 in cytosolic sensing of
543 SARS-CoV-2 RNAs (80, 81), although the primary RNA sensor might be cell-type
544 dependent. For instance, recent studies have implicated MDA-5 as the primary viral RNA
545 sensor in lung epithelial cells (82), while other studies have found both MDA-5 and RIG-I
546 sense SARS-CoV-2 infection in Calu-3 cells (81, 83). Our results implicate both RIG-I and
547 MDA-5 in SARS-CoV-2 RNA sensing in macrophages, as knockdown of either RIG-I or
548 MDA-5 significantly attenuated inflammatory cytokine induction in CD169^{+} macrophages.
549 Despite previous studies suggesting that induction of IL-6 and TNFα might be MAVS-
550 independent (84), knock-down of MAVS abrogated viral RNA sensing and induction of
551 NF-κB-dependent inflammatory cytokines (IL-6, TNFα, IL-1β, IL-18) in productively
552 infected (ACE2^{+}) and abortively infected (CD169^{+}) macrophages. Thus, we propose a co-
553 sensing requirement of both RIG-I and MDA-5 for detecting viral replication intermediates
554 and a pivotal role of MAVS in signal transduction in non-productively infected CD169^{+}
555 macrophages. Intriguingly, induction of RIG-I/MDA-5/MAVS-dependent IFNβ and ISG
556 expression was muted compared to the robust upregulation of NF-kB-dependent pro-
557 inflammatory cytokines in SARS-CoV-2 infected CD169^{+} macrophages. Since RLR
558 relocalization to the mitochondrial, peroxisomal or ER membranes is thought to initiate
559 robust MAVS-dependent IRF3 activation (85-87), it is tempting to speculate that during
560 restricted SARS-CoV-2 infection and diminished expression of viral RNAs, cytosolic
561 retention or altered intracellular localization of RLRs might control the strength and
562 specificity of downstream responses and favor NF-kB-dependent proinflammatory
563 cytokine expression. Future studies will need to address spatiotemporal dynamics of RIG-
564 I/MDA-5/MAVS interactions upon SARS-CoV-2 RNA sensing in macrophages.

565 SARS-CoV-2 RNA infection of lung epithelial cells can contribute to innate immune
566 activation, inflammation, recruitment of inflammatory monocytes and macrophages to the
567 alveolar space, and activation of tissue-resident alveolar macrophages (80, 81). Alveolar
568 macrophages and airway epithelial cell-associated macrophages, which are uniquely
569 positioned as gatekeepers to intercept invading pathogens from the bronchiolar airways,
570 constitutively express CD169 (58, 88), an ISG, whose expression can be further induced
571 by type I and type III IFNs (39, 50, 51, 89). While therapeutic use of both type I and III
572 IFNs have been proposed, clinical benefit has proven inconclusive (90-92), presumably
573 related to timing of the IFN response. For instance, a delayed and persistent type I IFN
574 response without resolution has been correlated with disease severity and mortality in
575 patients with COVIID-19 (68). As was recently suggested (93), the pathological outcomes
576 associated with a delayed type I IFN response might be partly due to the type I IFN-
577 induced expression of SARS-CoV-2 entry receptors, such as CD169, in
578 monocytes/macrophages and increased virus uptake and amplification of inflammatory
579 responses.

580 Treatment of COVID-19 patients with remdesivir has been shown to significantly
581 shorten recovery time and reduce lower respiratory tract infections, despite having
582 minimal impact on viremia (94, 95). Notably, combination therapy with Baricitinib, an anti-
583 inflammatory drug led to further improvement in clinical status and significantly lowered
584 serious adverse events (96). Therefore, targeting macrophage-intrinsic innate immune
585 activation by either blocking macrophage-specific receptors which can mediate SARS-
586 CoV-2 uptake, or through administration of RIG-I/MDA-5 antagonists present a novel
587 therapeutic strategy for combating hyperinflammation in COVID-19 patients. However,
588 further research is needed to better understand the mechanisms of ACE2-independent

589 CD169-mediated SARS-CoV-2 infection of macrophages, the post-entry restrictions to
590 virus replication, and the viral determinants that trigger innate immune activation.

591

592 **Figure Legends**

593 **Figure 1. ACE2-independent SARS-CoV-2 entry in macrophages.**

594 (**A-B**) Representative ACE2 mRNA expression (**A**) and flow cytometry profiles showing
595 ACE2 surface expression (**B**) of HEK293T cells stably expressing ACE2 and primary
596 MDMs from multiple donors. (**C-D**) Parental (vector) and transduced (ACE2) HEK293T
597 cells (**C**) and primary MDMs from 3 donors (**D**) were infected with S-pseudotyped lentivirus
598 (20 ng based on $p24^{Gag}$), in the absence or presence of cathepsin inhibitor (E64D) or
599 TMPRSS2 inhibitor (Camostat), and infection was quantified by measuring luciferase
600 activity at day 3 post-infection. Mock: no virus added, DMSO: no-treatment. The means ±
601 SEM from at least 3 independent experiments are shown. *P*-values: paired t-test, two-
602 tailed comparing to vector control (**C**), or one-way ANOVA followed by the Dunnett's post-
603 test comparing to DMSO (**D**). ***: $p < 0.001$, ****: $p < 0.0001$, ns: not significant.

604

605 **Figure 2. CD169 is a SARS-CoV-2 attachment and entry factor in macrophages.**

606 (**A**) Binding of SARS-CoV-2 S protein (Wuhan isolate) to THP1 monocytes expressing wt
607 CD169, mutant CD169 (R116A), ACE2, or both wt CD169 and ACE2 (CD169/ACE2). (**B**)
608 THP1/PMA macrophages were infected with S-pseudotyped lentivirus (20 ng $p24^{Gag}$), and
609 infection was quantified by measuring luciferase activity at 3 dpi. Relative light units
610 (RLUs) from each cell line were normalized to no virus control (mock). The means ± SEM
611 are shown from at least five independent experiments. (**C**) Primary MDMs from three
612 donors overexpressing either CD169 or ACE2, or control were infected with S-

613 pseudotyped lentivirus (20 ng $p24^{Gag}$) for 3 days, followed by analysis of luciferase activity
614 in whole cell lysates. (**D**) Untransduced primary MDMs (representative of 3 donors) were
615 pre-treated with anti-CD169 mAb (20 µg/ml, 7D2), IgG1, or empty media for 30 min at 4°C
616 prior to infection with S-pseudotyped lentivirus (20 ng $p24^{Gag}$) for 3 days, followed by
617 analysis of luciferase activity. RLUs from each donor in each group were normalized to
618 no virus control (mock). The means ± SEM from at least 3 independent experiments are
619 shown. *P*-values: paired t-test, two-tailed (**A**), one-way ANOVA followed by the Dunnett's
620 post-test (**B**) or Tukey's post-test comparing to parental (THP1) cells (**C**) or each pre-
621 treatment condition (D). ***: $p < 0.001$, ****: $p < 0.0001$, ns: not significant.
622
623 **Figure 3. SARS-CoV-2 establishes restricted infection in $CD169^+$ macrophages.**
624 (**A-D**) Representative immunofluorescence images (100x) of THP1/PMA macrophages
625 infected with SARS-CoV-2 (MOI=1) and stained for nucleus (DAPI, blue), SARS-CoV-2
626 dsRNA (green), and SARS-CoV-2 nucleocapsid (red), at indicated timepoints post
627 infection. Images shown for each THP1 cell line; untransduced control (parental, **A**),
628 CD169-expressing (**B**), ACE2-expressing (**C**), and CD169/ACE2 double expressing (**D**).
629 Bar=25 µm. (**E-F**) Culture supernatants from SARS-CoV-2 infected THP1/PMA cells (**E**)
630 and primary MDMs (**F**) were harvested at 24 hpi and viral titers determined by $TCID_{50}$
631 assay. The means ± SEM from at least 3 independent experiments are shown. LOD: limit
632 of detection of assay.
633
634 **Figure 4. CD169-mediated SARS-CoV-2 infection of macrophages results in**
635 **restricted viral RNA expression.**

636 (**A**) Single molecule RNA FISH analysis for viral RNAs using ORF1a specific probe set
637 (labeled with Texas Red) and N specific probe set (labelled with TMR) in SARS-CoV-2
638 infected THP1/PMA macrophages (MOI=10, 24 hpi) (**B**) Percentage of infected cells
639 based on the presence of SARS-CoV-2 RNAs determined from 10-20 independent fields,
640 (representative field shown in **A**). Data are representative of 2 independent experiments.
641 Bar=25 μm. (**C-F**) THP1/PMA macrophages infected with SARS-CoV-2 (MOI=1) in the
642 absence (**C-D**) or presence (**E-F**) of remdesivir (RDV, 1 μM). Total RNA was harvested at
643 indicated times post-infection and expression of viral transcripts was quantified by RT-
644 qPCR. Replication kinetics of SARS-CoV-2 was quantified by (**C**) total N amplification
645 (values from each group normalized to mock (uninfected) or (**D**) negative strand genome
646 from strand-specific reverse-transcription and ORF1b amplification (mean Ct values for
647 each condition). Expression of total N mRNA (**E**) and Envelope sgRNA (**F**) transcripts in
648 THP1/PMA cells pretreated with RDV was analyzed at 24 hpi. Values from each group
649 normalized to mock (uninfected). (**G-H**) MDMs from multiple donors were infected with
650 SARS-CoV-2 (MOI=1), in the absence or presence of RDV (1 μM), and viral replication
651 kinetics analyzed by RT-qPCR at indicated timepoints for total N mRNA (**G**), Envelope
652 sgRNA (**H**) transcripts. The means ± SEM are shown from at least 3 independent
653 experiments, each symbol represents a different donor. Significant differences between
654 groups were determined by one-way ANOVA followed by the Dunnett's post-test (**E-F**),
655 comparing to control parental THP1 cells. *P*-values: *<0.1; **<0.01; ***<0.001; ****<0.0001.
656

657 **Figure 5. Restricted expression of SARS-CoV-2 gRNA and sgRNA induces pro-**
658 **inflammatory responses in non-productively infected macrophages**

659 (**A-B**) PMA-differentiated THP1 cells from parental (THP1) or those expressing CD169,
660 ACE2, or CD169/ACE2 were infected with SARS-CoV-2 (MOI=1, 24 hpi) in the absence
661 or presence of RDV (1 μM, 30 mins), and total RNA was quantified by RT-qPCR for pro-
662 inflammatory cytokines and ISGs. Values were normalized to mock-infected control for
663 each group. Fold-induction for indicated pro-inflammatory cytokines (**A**, top panel) and
664 ISGs (**A**, bottom panel) in the absence of RDV, or in the presence of RDV (**B**). (**C-F**)
665 Kinetics of pro-inflammatory cytokine/ISG mRNA expression in the absence of RDV in
666 parental (**C**), CD169-expressing (**D**), ACE2-expressing (**E**), and CD169/ACE2-expressing
667 (**F**) PMA-differentiated THP1 cells. (**G**) MDMs from multiple donors were infected with
668 SARS-CoV-2 (MOI=1, 24 hpi) and total RNA analyzed by RT-qPCR. MDMs were pre-
669 treated with DMSO (control) or RDV (1 μM, 30 mins) prior to infection, and fold-induction
670 of indicated cytokine mRNAs normalized to mock-infected controls from each donor. RDV:
671 Remdesivir, ISGs: interferon-stimulated genes. Minus sign represents DMSO, and plus
672 sign represents RDV pre-treatment. The means ± SEM from at least 3 independent
673 experiments are shown. Significant differences between groups were determined by one-
674 way ANOVA followed by the Dunnett's post-test between groups (**A**) or Tukey's multiple
675 comparisons test within groups (**B** and **G**), comparing to parental THP1 (**A**) or DMSO-
676 treated (**B**, **G**) in each group. *P*-values: *<0.1; **<0.01; ***<0.001; ****<0.0001, ns: not
677 significant.
678
679 **Figure 6. Cytosolic RNA sensing by RIG-I and MDA-5 is required for SARS-CoV-2**
680 **induced innate immune responses in macrophages**
681 (**A-B**) CD169-expressing THP1 monocytes were transduced with lentivectors expressing
682 shRNA against non-specific control (scramble), or specific sequences against STING,

683 UNC93B1, MAVS, RIG-I, and MDA-5. Knockdown of host proteins targeted by shRNAs
684 compared to scramble analyzed by RT-qPCR (**A**), and immune blotting (**B**). (**C-H**) CD169$^+$
685 THP1 cells with stable knockdown of target genes were PMA-differentiated and infected
686 with SARS-CoV-2 (MOI=1, 24 hpi), and total RNA was analyzed by RT-qPCR for total
687 nucleocapsid (gRNA) (**C**), sgRNA (Envelope) (**D**), and pro-inflammatory cytokines/ISGs,
688 IL6, TNFα, IL-1β and IFNλ1 (**E-F**), normalized to mock-infected controls for each group.
689 Each knockdown is represented by different colors as in **A**. The means ± SEM from 3
690 independent experiments are shown, and significant differences were determined by one-
691 way ANOVA followed by the Dunnett's post-test comparing to scramble THP1 (**C**-**D**), or
692 by two-way ANOVA followed by Bonferroni post-test comparing Mock to CoV-2$^+$ in each
693 group (**E**-**H**). *P*-values: *<0.1; **<0.01; ***<0.001; ****<0.0001), ns: not significant.
694
695 **Figure 7. MAVS is essential for SARS-CoV-2 RNA-induced inflammatory responses**
696 **in macrophages.**
697 (**A**) Parental (THP1) monocytes and those expressing CD169, ACE2, or CD169/ACE2
698 were transduced with lentivectors expressing shRNA against scrambled sequence (-), or
699 MAVS sequence (+), and knockdown of MAVS in each cell line analyzed by immune
700 blotting (**A**, left panel), and quantified (**A**, right panel). (**B-C**) THP1 monocytes with stable
701 MAVS knockdown were PMA-differentiated and infected with SARS-CoV-2 (MOI=1, 24
702 hpi), and total RNA analyzed by RT-qPCR for (**B**) total viral transcripts (nucleocapsid),
703 and (**C**) IL6, TNFα, IL-1β and IFNλ1 mRNA expression, normalized to mock-infected
704 controls for each group. The means ± SEM from 3 independent experiments are shown,
705 and significant differences were determined by one-way ANOVA followed by the Tukey-

706 Kramer post-test within groups (**B**, and **C**), or Dunnett's post-test between groups (**C**). *P*-
707 values: *<0.05; **<0.01; ***<0.001; ****<0.0001, ns: not significant.
708

709 ## Supplementary Figure Legends

710 **Figure S1. Expression of endogenous TMPRSS2 and Cathepsin-L in human**
711 **macrophages**

712 (**A-B**) Western blot analysis for total TMPRSS2 (**A**) and Cathepsin-L (**B**) expression in
713 wildtype and transduced HT-29 cells (control), HEK293T, THP-1/PMA, and primary MDMs
714 from multiple donors. β-actin was probed as a loading control.
715

716 **Figure S2. Infection of primary MDMs by S-pseudotyped lentivirus is blocked by**
717 **anti-SARS-CoV-2 NTD antibodies.**

718 SARS-CoV-2 S-pseudotyped lentivirus (20 ng) was pre-incubated with indicated anti-
719 Spike neutralizing antibodies for 30 mins at 37°C, followed by infection of primary MDMs
720 for 3 days. Relative infection quantified by luciferase activity from whole cell lysates. NT:
721 no-treatment with neutralizing antibody. Data are representative of 2 independent
722 experiments, from 3 different donors each. Mock: no virus added, PBS: no-pre-incubation
723 of virus with antibody. The means ± SEM are shown. *P*-values: one-way ANOVA followed
724 by the Dunnett's post-test comparing to untreated (PBS) control, *: $p < 0.05$, **: $p < 0.01$,
725 ***: $p < 0.001$, ****: $p < 0.0001$.
726

727 **Figure S3. Expression profiles of human CD169 and ACE2 in THP1 monocytes and**
728 **primary MDMs.**

729 (**A**) Representative flow cytometry profiles of different THP1 cell lines and primary
730 MDMs stained for surface expression of CD169 and ACE2. (**A**) Transduced THP1 cell
731 lines stably expressing wild type (wt) CD169, mutant (R116A) CD169, ACE2, or both wt
732 CD169 and ACE2. (**B**) Untransduced primary MDMs from multiple donors showing
733 differential expression of endogenous CD169. After 5-6 days of macrophage
734 differentiation, cells were either unstained or stained with anti-human CD169 antibody,
735 and surface expression analyzed by flow cytometry. (**C-D**) Representative flow
736 cytometry profiles of primary MDMs transduced with wt CD169 (**C**) or ACE2 (**D**)
737 lentiviruses compared to negative (vector only) control.
738
739 **Figure S4. Exogenous expression of ACE2 in primary MDMs rescues SARS-CoV-2**
740 **replication.**
741 Representative immunofluorescence images (20x) of primary MDMs infected with SARS-
742 CoV-2 (MOI=1) and stained for nucleus (DAPI, blue), and SARS-CoV-2 nucleocapsid
743 protein (red), at 24 hpi. Images from primary MDMs overexpressing either CD169 or ACE2
744 compared to vector-only control were captured and represent at least 3 independent
745 donors. Bar = 25 μm.
746
747 **Figure S5. CD169 and ACE2-dependent temporal enhancement of SARS-CoV-2**
748 **RNAs in THP1/PMA macrophages.**
749 Single molecule FISH analysis of viral +gRNA using high fidelity probes in SARS-CoV-2
750 (MOI=10) infected THP1/PMA macrophages at the indicated timepoints. Representative
751 fields of cells were hybridized at indicated times with 7 sets of smFISH probes labeled

752 with Quasar670 targeting the + strand of SARS-CoV-2 ORF1a (NSP1-3) and N
753 transcripts. Data are representative of 2 independent experiments. Bar = 50μM
754
755 **Figure S6. Lack of pro-inflammatory cytokine expression in THP1/PMA**
756 **macrophages infected with SARS-CoV-2 S-pseudotyped lentiviruses.**
757 PMA-differentiated THP1 cell lines infected with SARS-CoV-2 S-pseudotyped lentivirus
758 (20 ng) and total RNA harvested at 2 dpi, followed by qRT-PCR analysis. Fold expression
759 of indicated cytokines normalized to mock (uninfected) condition in each group. Data are
760 representative of at least 3 independent experiments. The means ± SEM from 3
761 independent experiments are shown.
762

763 **Materials & Methods**

764 **Ethics statement.** This research has been determined to be exempt by the Institutional
765 Review Board of the Boston University Medical Center since it does not meet the definition
766 of human subjects research, since all human samples were collected in an anonymous
767 fashion and no identifiable private information was collected.

768

769 **Plasmids**

770 The SARS-CoV-2 S/gp41 expression plasmid was a gift from Dr. Nir Hachoen at the Broad
771 Institute, and has previously been described (74). For ACE2 lentiviral transduction in
772 THP1 cells, we used a lentiviral plasmid expressing ACE2 and the puromycin resistant
773 gene (Addgene #145839, hereafter pLenti-ACE2-IRES-puro). Generation of wildtype and
774 mutant (R116A) human CD169 plasmids (LNC-CD169) was previously described and
775 validated (39). For transduction of primary MDMs, a 3' LTR-restored lentiviral expression
776 vector (Addgene #101337, hereafter LV-3'LTR) expressing a GFP reporter was used to
777 express ACE2 or CD169. For ACE2 cloning, the NotI-XhoI fragment from pLenti-ACE2-
778 IRES-puro was inserted into the LV-3'LTR backbone. For cloning CD169 into LV-3'LTR
779 vector, a BglII-AgeI fragment from LNC-CD169 was inserted into LV-3'LTR vector. HIV-1
780 packaging plasmid psPAX2 and VSV-G expression constructs have been previously
781 described (39). All lentiviral vectors (pLKO.1) expressing shRNAs used for knockdown of
782 host proteins were purchased from Sigma.

783

784 **Cells**

785 HEK293T cells (ATCC) were maintained in DMEM (Gibco) containing 10% heat-
786 inactivated fetal bovine serum (FBS) (Gibco) and 1% pen/strep (Gibco) (39, 40, 97). Vero

787 E6 cells (ATCC CRL-1586) were maintained in DMEM supplemented with 10% FBS and
788 100 µg/mL primocin. THP1 cells (ATCC) were maintained in RPMI/1640 (Gibco)
789 containing 10% FBS and 1% pen/strep (50). THP1 cells stably expressing CD169 have
790 previously been described (39). To generate HEK293T/ACE2$^+$, THP1/ACE2$^+$ and
791 THP1/CD169$^+$/ACE2$^+$ cells, HEK293T, THP1 or THP1/CD169 cells were transduced with
792 pLenti-ACE2-IRES-puro lentivector and cultured in puromycin-containing media (2 µg/ml).
793 Cells with robust surface expression of ACE2 and CD169/ACE2 (double-positive) were
794 sorted using a MoFlo cell sorter (Beckman Coulter) and cultured in puromycin-
795 supplemented media. All cell lines are routinely tested for mycoplasma contamination and
796 confirmed negative. For THP1 monocyte to macrophage differentiation, THP1 cells were
797 stimulated with 100 nM PMA (Sigma-Aldrich) for 48 hours. Human monocyte-derived
798 macrophages (MDMs) were derived from CD14$^+$ peripheral blood monocytes by culturing
799 cells in RPMI/1640 (Gibco) media containing 10% heat-inactivated human AB serum
800 (Sigma-Aldrich) and recombinant human M-CSF (20 ng per ml; Peprotech) for 5-6 days,
801 (55). To generate MDMs expressing ACE2 or overexpressing CD169, cells were co-
802 infected with ACE2 or CD169 expressing lentiviruses (100 ng based on p24^{gag} ELISA per
803 1x10^6 cells) and SIV3+ (Vpx expressing) VLPs. ACE2 and CD169 surface expression was
804 determined by flow cytometry 3 days post transduction.
805
806 **Viruses**
807 SARS-CoV-2 stocks (isolate USA_WA1/2020, kindly provided by CDC's Principal
808 Investigator Natalie Thornburg and the World Reference Center for Emerging Viruses and
809 Arboviruses (WRCEVA)) were grown in Vero E6 cells (ATCC CRL-1586) cultured in
810 Dulbecco's modified Eagle's medium (DMEM) supplemented with 2% fetal FBS and 100

811 μg/mL primocin. To remove confounding cytokines and other factors, viral stocks were
812 purified by ultracentrifugation through a 20% sucrose cushion at 80,000xg for 2 hours at
813 4°C (60). SARS-CoV-2 titer was determined in Vero E6 cells by tissue culture infectious
814 dose 50 ($TCID_{50}$) assay using the Spearman Kärber algorithm. All work with SARS-CoV-
815 2 was performed in the biosafety level 4 (BSL4) facility of the National Emerging Infectious
816 Diseases Laboratories at Boston University, Boston, MA following approved SOPs.
817 Generation of SARS-CoV-2 S-pseudotyped lentiviruses expressing spike glycoprotein
818 has previously been described (74). Briefly, HEK293T cells were co-transfected with HIV-
819 1 reporter plasmid containing a luciferase reporter gene in place of the *nef* ORF and
820 SARS-CoV-2 S (74). To generate ACE2 or CD169 expressing recombinant lentiviruses,
821 LV-3'LTR lentivectors expressing either empty vector, ACE2, or CD169, were co-
822 transfected with psPax2 (HIV Gag-pol packaging plasmid) and H-CMV-G (VSV-G
823 envelope-expressing plasmid) in HEK293T cells by calcium phosphate-mediated
824 transfection (98). Virus-containing supernatants were harvested 2 days post-transfection,
825 cleared of cell debris by centrifugation (300xg, 5 min), passed through 0.45 μm filters,
826 aliquoted and stored at -80 °C until use. Lentivirus titers were determined by a $p24^{gag}$
827 ELISA (98).
828
829 **Infection**
830 For RNA analysis, $1x10^6$ cells (THPI/PMA, MDMs, HEK293T) were seeded in 12-well
831 plates. For smFISH analysis, $1x10^6$ cells were seeded in 6-well plates containing 3-4
832 coverslips per well. The next day, cells were infected with purified SARS-CoV-2 at the
833 indicated multiplicity of infection (MOI). At indicated time points, the cells were either lysed
834 with TRIzol (for total RNA analysis) or fixed in 10% neutral buffered formalin for at least 6

835 hours at 4°C and removed from the BSL-4 laboratory for staining and imaging analysis in
836 accordance with approved SOPs. For SARS-CoV-2 S-pseudotyped lentiviral infections of
837 THP1/PMA macrophages or MDMs, $1x10^5$ cells were seeded in 96-well plates, and
838 infected via spinoculation the following day with 10-20 ng ($p24^{Gag}$) of purified S-
839 pseudotyped lentivirus and SIV_{mac} Vpx VLPs (1 hr at RT and 1100 x g), as previously
840 described (55). Incubation with virus was continued for 4 additional hours at 37˚C, cells
841 were then washed to remove unbound virus particles, and cultured for 2-3 days. For
842 CD169 blocking experiments, primary MDMs from 3 different donors were pre-incubated
843 with 20 µg/ml anti-CD169 antibody (HSn 7D2, Novus Biologicals) or IgG1k (P3.6.2.8.1,
844 eBioscience) for 30 min at 4˚C prior to infection. For anti-spike neutralizing experiments,
845 virus-containing media were pre-incubated with antibodies targeting SARS-CoV-2 spike
846 NTD for 30 min at 37˚C prior to infection. At indicated timepoints, cells are lysed, cell
847 lysates were analyzed for luciferase activity using the Bright-Glo luciferase assay kit
848 (Promega), as previously described (36). The SARS-CoV-2 neutralizing antibodies was
849 previously characterized (57) and were a kind gift from Dr. Duane Wesemann at Harvard
850 Medical School.
851
852 **S binding**
853 To evaluate SARS-CoV-2 S binding to various THP1 monocytes expressing different
854 surface receptors, approximately $0.25x10^6$ cells from parental THP1 or those expressing
855 wt CD169, mutant CD169 (R116A), ACE2, or both wt CD169 and ACE2 were incubated
856 for 30 min at 4 °C with 2 µg of spike glycoprotein (stabilized) from Wuhan-Hu-1 SARS-
857 CoV-2 containing a C-terminal Histidine Tag, recombinant from HEK293F cells (BEI
858 resources, #NR-52397). This is followed by secondary staining for 30 min at 4˚C with

859 APC-conjugated mouse anti-His antibody (BioLegend, #362605, 1:50) or isotype control.
860 Cells were fixed with 4% PFA (Boston Bioproducts) for 30 min, and analyzed with BD
861 LSRII (BD). Data analysis was performed using FlowJo software (FlowJo).
862
863 **Immunofluorescence**
864 In brief, the cells were permeabilized with acetone-methanol solution (1:1) for 10 min at -
865 20°C, incubated in 0.1 M glycine for 10 min at room temperature and subsequently
866 incubated in 5% goat serum (Jackson ImmunoResearch) for 20 minutes at room
867 temperature. After each step, the cells were washed three times in PBS. The cells were
868 incubated overnight at 4°C with a rabbit antibody directed against the SARS-CoV
869 nucleocapsid protein (Rockland; 1:1000 dilution in 5% goat serum), which cross-reacts
870 with the SARS-CoV-2 nucleocapsid protein, as previously described (99). The cells were
871 washed four times in PBS and incubated with goat anti-rabbit antibody conjugated with
872 AlexaFluor594 for 1 hour at room temperature (Invitrogen; 1:200 dilution in blocking
873 reagent). 4',6-diamidino-2-phenylindole (DAPI; Sigma-Aldrich) was used at 200 ng/ml for
874 nuclei staining. For dsRNA staining (61), anti-dsRNA (Pan-Enterovirus Reagent, clone
875 9D5, Light Diagnostics, Millipore) antibody was used 1:2 overnight and anti-mouse-AF488
876 (Invitrogen) 1:200 dilution as secondary antibody with DAPI. Images were acquired using
877 a Nikon Eclipse Ti2 microscope with Photometrics Prime BSI camera and NIS Elements
878 AR software.
879
880 **RNA isolation and RT-qPCR**
881 Total RNA was isolated from infected cells using TRIzol reagent (Invitrogen). Reverse
882 transcription (RT) from purified RNAs was performed using oligo$(dT)_{20}$ primer (Superscript

883 III, Invitrogen) or strand-specific RT primers as previously described (100). Target mRNAs
884 were quantified using Maxima SYBR Green (Thermo Scientific), using the primer sets
885 shown in **Table 1**. Primer sequences for GAPDH, IL-6, TNFα, IL-1β, IP-10, IFNλ1, IL-18,
886 Viperin and IFNβ have been described previously (97). The C_T value was normalized to
887 that of GAPDH and represented as a relative value to a 'mock' control using the $2^{-\Delta\Delta C_T}$
888 method as described (97, 101).
889
890 **shRNA mediated knockdown**
891 Stable knockdown of host proteins in THP1 cells was carried out by transduction with
892 lentivectors expressing individual shRNAs (pLKO.1, 400 ng $p24^{Gag}$ (as measured by
893 ELISA) per 1×10^6 cells) in the presence of polybrene (Millipore). Cells were washed and
894 cultured for 5-7 days in the presence of puromycin (2 µg/ml, InvivoGen). Selected cells
895 were expanded, and knockdown confirmed and quantified by RT-qPCR or western
896 blotting, prior to any downstream experiments. All shRNA target sequences are listed in
897 **Table 2**.
898
899 **Flow cytometry**
900 To examine cell surface expression of CD169 or ACE2 in transduced THP1 or primary
901 MDMs, approximately 0.5×10^6 cells were harvested with CellStripper (Corning), stained
902 with Zombie-NIR (BioLegend, #423105, 1:250) followed by staining for 30 min at 4˚C with
903 the following antibodies; Alexa647-conjugated mouse anti-CD169 antibody (BioLegend,
904 #346006, 1:50), Alexa647-conjugated mouse anti-ACE2 antibody (R&D systems, 1:200),
905 or unconjugated goat anti-ACE2 polyclonal antibody (R&D systems, #AF933, 1:200)
906 followed by Alexa488-conjugated chicken anti-goat antibody (Invitrogen, #A-21467,

907 1:100). Cells were fixed with 4% PFA (Boston Bioproducts) for 30 min, and analyzed with
908 BD LSRII (BD). Data analysis was performed using FlowJo software (FlowJo).
909
910 **smFISH**
911 *Probe designs*. smFISH probes used to detect different RNA segments of the SARS-CoV-
912 2 genome (NCBI reference sequence: NC_045512.2) consisted of a set of 48
913 oligonucleotides, each with length of 20 nt and labeled with different fluorophores (*see*
914 *Table. 3 in supplementary information*) for target genes and sequences for each of the
915 probe sets). Probes were designed using Stellaris™ Probe Designer by LGC Biosearch
916 Technologies and purchased from Biosearch Technologies. The 3'-end of each probe was
917 modified with an amine group and coupled to either tetramethylrhodamine (TMR; Thermo
918 Fisher Scientific), Texas Red-X (Thermo Fisher Scientific), Quasar 670 (Biosearch
919 Technologies) or Cy5 (Lumiprobe). Coupled probes were ethanol precipitated and purified
920 on an HPLC column to isolate oligonucleotides linked to the fluorophore via their amine
921 groups, as previously described by *Raj et.al.* (62).
922 *Hybridization*. Cells were cultured on glass coverslips, fixed at appropriate times with 10%
923 neutral buffered formalin and permeabilized with 70% methanol. Coverslips were
924 equilibrated with hybridization wash buffer (10% formamide, 2X SSC), and then immersed
925 in 50 µL of hybridization buffer, which consisted of 10% dextran sulphate (Sigma-Aldrich),
926 1 mg/mL *Escherichia coli* transfer RNA (Sigma-Aldrich), 2 mM ribonucleoside vanadyl
927 complexes (New England Biolabs, Ipswich, MA), 0.02% ribonuclease-free bovine serum
928 albumin (Thermo Fisher Scientific), 10% formamide, 2X SSC, and conjugated probes with
929 appropriate concentration (25 ng of pooled probes). This hybridization reaction mixture
930 was first added as a droplet onto a stretched-out piece of Parafilm (Bemis in North

931 America, Oshkosh, WI) over a glass plate, and then a coverslip containing the cells was
932 placed faced down onto the droplet, followed by incubation at 37ºC overnight in a humid
933 chamber. Following hybridization, the coverslips were washed twice for 10 minutes each
934 in 1 mL of hybridization wash buffer at room temperature. The coverslips were then
935 equilibrated with mounting buffer (2X SCC, 0.4% glucose) and mounted in the mounting
936 buffer supplemented with 1 µL of 3.7 mg/mL glucose oxidase and 1 µL of catalase
937 suspension (both from Sigma-Aldrich) for each 100 µL preparation. After removing the
938 excess mounting medium by gently blotting with a tissue paper, the coverslips were sealed
939 with clear nail polish, and then imaged on the same day.
940 *Image acquisition, pre-processing, analysis and mRNA quantification.* Images were
941 acquired using Zeiss Axiovert 200M (63x oil immersion objective; numerical aperture 1.4)
942 controlled by Metamorph image acquisition software (Molecular Devices, San Jose, CA).
943 Stacks of images of 16 layers with 0.2 µm interval at 100- to 2,000-milisecond exposure
944 times were used in each fluorescence color channel including DAPI. Two representative
945 coverslips per sample/group were selected and 10-20 regions/fields of interest were
946 imaged. For cell fluorescence intensity measurements, region of interest was drawn
947 manually around each cell using DIC and DAPI channels, then average intensity was
948 measure within the area of each cell using RNA-specific florescence channels.
949
950 **Immunoblot Analysis**
951 To assess expression of endogenous or transduced proteins, cell lysates containing 30-
952 40 µg total protein were separated by SDS-PAGE, transferred to nitrocellulose
953 membranes and the membranes were probed with the following antibodies: mouse anti-
954 TMPRSS2 (Santa Cruz, #515727, 1:1000), mouse anti-Cathepsin-L (Santa Cruz,

955 #32320, 1:1000), goat anti-ACE-2 (R&D systems, #AF933, 1;1000), rabbit anti-STING
956 (Cell Signaling, #13647, 1:1000), rabbit anti-MAVS (Thermo Fisher, #PA5-17256,
957 1:1000), mouse anti-RIG-I (AdipoGen, #20B-0009, 1:1000), rabbit anti-MDA-5
958 (Proteintech, #21775-1-AP, 1:1000), rabbit anti-UNC93B1 (Invitrogen, #PA5-83437,
959 1:1000), rabbit anti-IRF1 (Cell Signaling, #8478S, 1:1000). Specific staining was
960 visualized with secondary antibodies, goat anti-mouse-IgG-DyLight 680 (Thermo
961 Scientific, #35518, 1:20000), goat anti-rabbit-IgG-DyLight 800 (Thermo Scientific, #SA5-
962 35571, 1:20000), or a donkey anti-goat-IgG-IR-Dye 800 (Licor, #926-32214, 1:20000).
963 As loading controls, actin or tubulin expression was probed using a rabbit anti-actin
964 (Sigma-Aldrich, A2066, 1:5000), mouse anti-actin (Invitrogen, #AM4302, 1:5000), or
965 rabbit anti-tubulin (Cell Signaling, #3873, 1;5000). Membranes were scanned with an
966 Odessy scanner (Li-Cor).
967
968 **Statistics**
969 All the statistical analysis was performed using GraphPad Prism 9. *P*-values were
970 calculated using one-way ANOVA followed by the Tukey-Kramer post-test (symbols for *p*-
971 values shown with a line) or the Dunnett's post-test (comparing to mock), symbols for *p*-
972 values shown with a bracket), or a two-tailed paired t-test (comparing two samples,
973 symbols for two-tailed *p*-values shown with a line bracket). Symbols represent, *: $p < 0.05$,
974 **: $p < 0.01$, ***: $p < 0.001$, ****: $p < 0.0001$. No symbol or ns: not significant ($p \geq 0.05$).
975
976 **Data availability**
977 The authors declare that the data that support the findings of this study are available within
978 the paper and from the corresponding author upon reasonable request.

979

980 **Table 1**

981 **qRT-PCR primers:**

Gene	Forward	Reverse
GAPDH	CAAGATCATCAGCAATGCCT	AGGGATGATGTTCTGGAGAG
IL-6	TCTCCACAAGCGCCTTCG	CTCAGGGCTGAGATGCCG
TNFα	CCCAGGGACCTCTCTCTAATCA	GCTACAGGCTTGTCACTCGG
IL-1β	AAACAGATGAAGTGCTCCTTCC	AAGATGAAGGGAAAGAAGGTGC
IL-18	GACCAAGGAAATCGGCCTCTA	ACCTCTAGGCTGGCTATCTTTATACATAC
IFNβ	ATTCTAACTGCAACCTTTCG	GTTGTAGCTCATGGAAAGAG
IP-10	AAAGCAGTTAGCAAGGAAAG	TCATTGGTCACCTTTTAGTG
Viperin	TGGGTGCTTACACCTGCTG	GAAGTGATAGTTGACGCTGGTT
IFNλ1	GGACGCCTTGGAAGAGTCAC	AGCTGGGAGAGGATGTGGT
SARS-CoV-2_ negative strand	ACAGCACCCTAGCTTGGTAGCCGAACAACTGGACTTTATTGA	
nCoVsg_E.rtF	CGAACTTATGTACTCATTCGTTTCGG	
nCoVsg_E.rtR	AGAAGGTTTTACAAGACTCACGTT	
SARS-CoV-2 Nucleocapsid	CACATTGGCACCCGCAATC	GAGGAACGAGAAGAGGCTTG
SARS-CoV-2 Envelope (E)	ACAGGTACGTTAATAGTTAATAGCGT	ATATTGCAGCAGTACGCACACA
TRS 5' leader (forward)	ACCAACCAACTTTCGATCTCTTGT	
N 3' reverse	CACTGCGTTCTCCATTCTGG	
ACE-2	CGAAGCCGAAGGCCTGTTCTA	GGGCAAGTGTGGACTGTTCC
TMPRSS2	CAAGTGCTCCAACTCTGGGAT	AACACACCGATTCTCGTCCTC
STING	ACTGTGGGGTGCCTGATAAC	TGGCAAACAAAGTCTGCAAG
MAVS	GTACCCGAGTCTCGTTTC	GCAGAATCTCTACAACATCC
RIG-I	ATCCCAGTGTATGAACAGCAG	GCCTGTAACTCTATACCCATGTC
MDA-5	GGCATGGAGAATAACTCATCAG	CTCTTCATCTGAATCACTTCCC
UNC93B1	TGATCCTGCACTACGACGAG	GCGAGGAACATCATCCACTT

982

983 **Table 2**

984 **shRNA sequences:**

Gene	Sequence	Reference
STING	GCCCGGATTCGAACTTACAAT	Sigma (TRCN0000163296)

MAVS	ATGTGGATGTTGTAGAGATTC	Sigma (TRCN0000236031)
RIG-I	CCAGAATTATCCCAACCGATA	Sigma (TRCN0000153712)
MDA-5	CCAACAAAGAAGCAGTGTATA	Sigma (TRCN0000050849)
UNC93B1	CAAGGAGAGACAGGACTTCAT	Sigma (TRCN0000138268)

985

986 **Table 3**

987 **smFISH probe sequences:**

988 See attached excel sheet.

989

990 ## Acknowledgments

991 We thank the BUMC Flow Cytometry Core, the Cellular Imaging Core, and Mitchell
992 White, BU for technical assistance. We are grateful to Robert Davey, BU for help with
993 imaging. This work was supported by NIH grants R01AI064099 (SG), R01DA051889
994 (SG), R01AG060890 (SG), P30AI042853 (SG), R01CA2 27292 (ST), R01AI106036 (YB
995 and ST), R01AI133486 (EM), and R21AI135912 (EM) as well as Fast Grants (EM) and
996 Evergrande MassCPR (EM). The funders had no role in study design, data collection
997 and analysis, decision to publish, or preparation of the manuscript.

998

999

1000 ## Author Contributions

1001 S.J., J.O., E.M. and S.G. designed the experiments. S.J., J.O, J.B., A.N., E.L., M.L., H.A.,
1002 Y.B., and S.T., performed the experiments and analyzed the data. S.J., J.O., E.M. and
1003 S.G. wrote the manuscript.

1004

1005 **References**

1006 1. Del Valle DM, Kim-Schulze S, Huang HH, Beckmann ND, Nirenberg S, Wang B,
1007 et al. An inflammatory cytokine signature predicts COVID-19 severity and
1008 survival. *Nat Med.* 2020;26(10):1636-43.
1009 2. Zhou F, Yu T, Du R, Fan G, Liu Y, Liu Z, et al. Clinical course and risk factors for
1010 mortality of adult inpatients with COVID-19 in Wuhan, China: a retrospective
1011 cohort study. *Lancet.* 2020;395(10229):1054-62.
1012 3. Chen G, Wu D, Guo W, Cao Y, Huang D, Wang H, et al. Clinical and
1013 immunological features of severe and moderate coronavirus disease 2019. *J Clin*
1014 *Invest.* 2020;130(5):2620-9.
1015 4. Ruan Q, Yang K, Wang W, Jiang L, and Song J. Clinical predictors of mortality
1016 due to COVID-19 based on an analysis of data of 150 patients from Wuhan,
1017 China. *Intensive Care Med.* 2020;46(5):846-8.
1018 5. Pugin J, Ricou B, Steinberg KP, Suter PM, and Martin TR. Proinflammatory
1019 activity in bronchoalveolar lavage fluids from patients with ARDS, a prominent
1020 role for interleukin-1. *Am J Respir Crit Care Med.* 1996;153(6 Pt 1):1850-6.
1021 6. Giamarellos-Bourboulis EJ, Netea MG, Rovina N, Akinosoglou K, Antoniadou A,
1022 Antonakos N, et al. Complex Immune Dysregulation in COVID-19 Patients with
1023 Severe Respiratory Failure. *Cell Host Microbe.* 2020;27(6):992-1000 e3.
1024 7. Zhou Z, Ren L, Zhang L, Zhong J, Xiao Y, Jia Z, et al. Heightened Innate Immune
1025 Responses in the Respiratory Tract of COVID-19 Patients. *Cell Host Microbe.*
1026 2020;27(6):883-90 e2.
1027 8. Liao M, Liu Y, Yuan J, Wen Y, Xu G, Zhao J, et al. Single-cell landscape of
1028 bronchoalveolar immune cells in patients with COVID-19. *Nat Med.*
1029 2020;26(6):842-4.
1030 9. Wen W, Su W, Tang H, Le W, Zhang X, Zheng Y, et al. Immune cell profiling of
1031 COVID-19 patients in the recovery stage by single-cell sequencing. *Cell Discov.*
1032 2020;6(1):31.
1033 10. Abdelmoaty MM, Yeapuri P, Machhi J, Olson KE, Shahjin F, Kumar V, et al.
1034 Defining the Innate Immune Responses for SARS-CoV-2-Human Macrophage
1035 Interactions. *Front Immunol.* 2021;12:741502.
1036 11. Boumaza A, Gay L, Mezouar S, Bestion E, Diallo AB, Michel M, et al. Monocytes
1037 and Macrophages, Targets of Severe Acute Respiratory Syndrome Coronavirus
1038 2: The Clue for Coronavirus Disease 2019 Immunoparalysis. *J Infect Dis.*
1039 2021;224(3):395-406.
1040 12. Garcia-Nicolas O, V'Kovski P, Zettl F, Zimmer G, Thiel V, and Summerfield A. No
1041 Evidence for Human Monocyte-Derived Macrophage Infection and Antibody-
1042 Mediated Enhancement of SARS-CoV-2 Infection. *Front Cell Infect Microbiol.*
1043 2021;11:644574.
1044 13. Junqueira C, Crespo A, Ranjbar S, Ingber J, Parry B, Ravid S, et al. SARS-CoV-2
1045 infects blood monocytes to activate NLRP3 and AIM2 inflammasomes, pyroptosis
1046 and cytokine release. *medRxiv.* 2021.
1047 14. Rodrigues TS, de Sa KSG, Ishimoto AY, Becerra A, Oliveira S, Almeida L, et al.
1048 Inflammasomes are activated in response to SARS-CoV-2 infection and are
1049 associated with COVID-19 severity in patients. *J Exp Med.* 2021;218(3).
1050 15. Zheng J, Wang Y, Li K, Meyerholz DK, Allamargot C, and Perlman S. Severe
1051 Acute Respiratory Syndrome Coronavirus 2-Induced Immune Activation and

1052 Death of Monocyte-Derived Human Macrophages and Dendritic Cells. *J Infect*
1053 *Dis.* 2021;223(5):785-95.
1054 16. Lempp FA, Soriaga LB, Montiel-Ruiz M, Benigni F, Noack J, Park YJ, et al.
1055 Lectins enhance SARS-CoV-2 infection and influence neutralizing antibodies.
1056 *Nature.* 2021;598(7880):342-7.
1057 17. Lu Q, Liu J, Zhao S, Gomez Castro MF, Laurent-Rolle M, Dong J, et al. SARS-
1058 CoV-2 exacerbates proinflammatory responses in myeloid cells through C-type
1059 lectin receptors and Tweety family member 2. *Immunity.* 2021;54(6):1304-19 e9.
1060 18. Moore JB, and June CH. Cytokine release syndrome in severe COVID-19.
1061 *Science.* 2020;368(6490):473-4.
1062 19. Perez-Zsolt D, Munoz-Basagoiti J, Rodon J, Elosua-Bayes M, Raich-Regue D,
1063 Risco C, et al. SARS-CoV-2 interaction with Siglec-1 mediates trans-infection by
1064 dendritic cells. *Cell Mol Immunol.* 2021;18(12):2676-8.
1065 20. Delorey TM, Ziegler CGK, Heimberg G, Normand R, Yang Y, Segerstolpe A, et
1066 al. COVID-19 tissue atlases reveal SARS-CoV-2 pathology and cellular targets.
1067 *Nature.* 2021;595(7865):107-13.
1068 21. Grant RA, Morales-Nebreda L, Markov NS, Swaminathan S, Querrey M, Guzman
1069 ER, et al. Circuits between infected macrophages and T cells in SARS-CoV-2
1070 pneumonia. *Nature.* 2021;590(7847):635-41.
1071 22. Bost P, Giladi A, Liu Y, Bendjelal Y, Xu G, David E, et al. Host-Viral Infection
1072 Maps Reveal Signatures of Severe COVID-19 Patients. *Cell.* 2020;181(7):1475-
1073 88 e12.
1074 23. Tang L, Yin Z, Hu Y, and Mei H. Controlling Cytokine Storm Is Vital in COVID-19.
1075 *Front Immunol.* 2020;11:570993.
1076 24. Sefik E, Qu R, Kaffe E, Zhao J, Junqueira C, Mirza H, et al. Viral replication in
1077 human macrophages enhances an inflammatory cascade and interferon driven
1078 chronic COVID-19 in humanized mice. *bioRxiv.* 2021.
1079 25. Hoffmann M, Kleine-Weber H, and Pohlmann S. A Multibasic Cleavage Site in
1080 the Spike Protein of SARS-CoV-2 Is Essential for Infection of Human Lung Cells.
1081 *Mol Cell.* 2020;78(4):779-84 e5.
1082 26. Hoffmann M, Kleine-Weber H, Schroeder S, Kruger N, Herrler T, Erichsen S, et
1083 al. SARS-CoV-2 Cell Entry Depends on ACE2 and TMPRSS2 and Is Blocked by
1084 a Clinically Proven Protease Inhibitor. *Cell.* 2020;181(2):271-80 e8.
1085 27. Lu R, Zhao X, Li J, Niu P, Yang B, Wu H, et al. Genomic characterisation and
1086 epidemiology of 2019 novel coronavirus: implications for virus origins and
1087 receptor binding. *Lancet.* 2020;395(10224):565-74.
1088 28. Xia S, Lan Q, Su S, Wang X, Xu W, Liu Z, et al. The role of furin cleavage site in
1089 SARS-CoV-2 spike protein-mediated membrane fusion in the presence or
1090 absence of trypsin. *Signal Transduct Target Ther.* 2020;5(1):92.
1091 29. Zang R, Gomez Castro MF, McCune BT, Zeng Q, Rothlauf PW, Sonnek NM, et
1092 al. TMPRSS2 and TMPRSS4 promote SARS-CoV-2 infection of human small
1093 intestinal enterocytes. *Sci Immunol.* 2020;5(47).
1094 30. Hikmet F, Mear L, Edvinsson A, Micke P, Uhlen M, and Lindskog C. The protein
1095 expression profile of ACE2 in human tissues. *Mol Syst Biol.* 2020;16(7):e9610.
1096 31. Sungnak W, Huang N, Becavin C, Berg M, Queen R, Litvinukova M, et al. SARS-
1097 CoV-2 entry factors are highly expressed in nasal epithelial cells together with
1098 innate immune genes. *Nat Med.* 2020;26(5):681-7.

1099 32. Beers C, Honey K, Fink S, Forbush K, and Rudensky A. Differential regulation of
1100 cathepsin S and cathepsin L in interferon gamma-treated macrophages. *J Exp*
1101 *Med.* 2003;197(2):169-79.
1102 33. Szulc-Dabrowska L, Bossowska-Nowicka M, Struzik J, and Toka FN. Cathepsins
1103 in Bacteria-Macrophage Interaction: Defenders or Victims of Circumstance? *Front*
1104 *Cell Infect Microbiol.* 2020;10:601072.
1105 34. Jeffers SA, Tusell SM, Gillim-Ross L, Hemmila EM, Achenbach JE, Babcock GJ,
1106 et al. CD209L (L-SIGN) is a receptor for severe acute respiratory syndrome
1107 coronavirus. *Proc Natl Acad Sci U S A.* 2004;101(44):15748-53.
1108 35. Marzi A, Gramberg T, Simmons G, Moller P, Rennekamp AJ, Krumbiegel M, et al.
1109 DC-SIGN and DC-SIGNR interact with the glycoprotein of Marburg virus and the
1110 S protein of severe acute respiratory syndrome coronavirus. *J Virol.*
1111 2004;78(21):12090-5.
1112 36. Akiyama H, Ramirez NG, Gudheti MV, and Gummuluru S. CD169-mediated
1113 trafficking of HIV to plasma membrane invaginations in dendritic cells attenuates
1114 efficacy of anti-gp120 broadly neutralizing antibodies. *PLoS Pathog.*
1115 2015;11(3):e1004751.
1116 37. Gummuluru S, Pina Ramirez NG, and Akiyama H. CD169-dependent cell-
1117 associated HIV-1 transmission: a driver of virus dissemination. *J Infect Dis.*
1118 2014;210 Suppl 3:S641-7.
1119 38. Izquierdo-Useros N, Lorizate M, Puertas MC, Rodriguez-Plata MT, Zangger N,
1120 Erikson E, et al. Siglec-1 is a novel dendritic cell receptor that mediates HIV-1
1121 trans-infection through recognition of viral membrane gangliosides. *PLoS Biol.*
1122 2012;10(12):e1001448.
1123 39. Puryear WB, Akiyama H, Geer SD, Ramirez NP, Yu X, Reinhard BM, et al.
1124 Interferon-inducible mechanism of dendritic cell-mediated HIV-1 dissemination is
1125 dependent on Siglec-1/CD169. *PLoS Pathog.* 2013;9(4):e1003291.
1126 40. Akiyama H, Miller C, Patel HV, Hatch SC, Archer J, Ramirez NG, et al. Virus
1127 particle release from glycosphingolipid-enriched microdomains is essential for
1128 dendritic cell-mediated capture and transfer of HIV-1 and henipavirus. *J Virol.*
1129 2014;88(16):8813-25.
1130 41. Izquierdo-Useros N, Lorizate M, Contreras FX, Rodriguez-Plata MT, Glass B,
1131 Erkizia I, et al. Sialyllactose in viral membrane gangliosides is a novel molecular
1132 recognition pattern for mature dendritic cell capture of HIV-1. *PLoS Biol.*
1133 2012;10(4):e1001315.
1134 42. Perez-Zsolt D, Erkizia I, Pino M, Garcia-Gallo M, Martin MT, Benet S, et al. Anti-
1135 Siglec-1 antibodies block Ebola viral uptake and decrease cytoplasmic viral entry.
1136 *Nat Microbiol.* 2019;4(9):1558-70.
1137 43. Puryear WB, Yu X, Ramirez NP, Reinhard BM, and Gummuluru S. HIV-1
1138 incorporation of host-cell-derived glycosphingolipid GM3 allows for capture by
1139 mature dendritic cells. *Proc Natl Acad Sci U S A.* 2012;109(19):7475-80.
1140 44. Kijewski SDG, Akiyama H, Feizpour A, Miller CM, Ramirez NP, Reinhard BM, et
1141 al. Access of HIV-2 to CD169-dependent dendritic cell-mediated trans infection
1142 pathway is attenuated. *Virology.* 2016;497:328-36.
1143 45. Watanabe Y, Allen JD, Wrapp D, McLellan JS, and Crispin M. Site-specific glycan
1144 analysis of the SARS-CoV-2 spike. *Science.* 2020;369(6501):330-3.
1145 46. Yang Q, Hughes TA, Kelkar A, Yu X, Cheng K, Park S, et al. Inhibition of SARS-
1146 CoV-2 viral entry upon blocking N- and O-glycan elaboration. *Elife.* 2020;9.

1147 47. Crocker PR, Paulson JC, and Varki A. Siglecs and their roles in the immune
1148 system. *Nat Rev Immunol.* 2007;7(4):255-66.
1149 48. Ducreux J, Crocker PR, and Vanbever R. Analysis of sialoadhesin expression on
1150 mouse alveolar macrophages. *Immunol Lett.* 2009;124(2):77-80.
1151 49. Oh DS, Oh JE, Jung HE, and Lee HK. Transient Depletion of CD169(+) Cells
1152 Contributes to Impaired Early Protection and Effector CD8(+) T Cell Recruitment
1153 against Mucosal Respiratory Syncytial Virus Infection. *Front Immunol.*
1154 2017;8:819.
1155 50. Akiyama H, Ramirez NP, Gibson G, Kline C, Watkins S, Ambrose Z, et al.
1156 Interferon-Inducible CD169/Siglec1 Attenuates Anti-HIV-1 Effects of Alpha
1157 Interferon. *J Virol.* 2017;91(21).
1158 51. Rempel H, Calosing C, Sun B, and Pulliam L. Sialoadhesin expressed on IFN-
1159 induced monocytes binds HIV-1 and enhances infectivity. *PLoS One.*
1160 2008;3(4):e1967.
1161 52. York MR, Nagai T, Mangini AJ, Lemaire R, van Seventer JM, and Lafyatis R. A
1162 macrophage marker, Siglec-1, is increased on circulating monocytes in patients
1163 with systemic sclerosis and induced by type I interferons and toll-like receptor
1164 agonists. *Arthritis Rheum.* 2007;56(3):1010-20.
1165 53. Doehn JM, Tabeling C, Biesen R, Saccomanno J, Madlung E, Pappe E, et al.
1166 CD169/SIGLEC1 is expressed on circulating monocytes in COVID-19 and
1167 expression levels are associated with disease severity. *Infection.* 2021;49(4):757-
1168 62.
1169 54. Lee JS, and Shin EC. The type I interferon response in COVID-19: implications
1170 for treatment. *Nat Rev Immunol.* 2020;20(10):585-6.
1171 55. Akiyama H, Miller CM, Ettinger CR, Belkina AC, Snyder-Cappione JE, and
1172 Gummuluru S. HIV-1 intron-containing RNA expression induces innate immune
1173 activation and T cell dysfunction. *Nat Commun.* 2018;9(1):3450.
1174 56. Afar DE, Vivanco I, Hubert RS, Kuo J, Chen E, Saffran DC, et al. Catalytic
1175 cleavage of the androgen-regulated TMPRSS2 protease results in its secretion
1176 by prostate and prostate cancer epithelia. *Cancer Res.* 2001;61(4):1686-92.
1177 57. Tong P, Gautam A, Windsor IW, Travers M, Chen Y, Garcia N, et al. Memory B
1178 cell repertoire for recognition of evolving SARS-CoV-2 spike. *Cell.*
1179 2021;184(19):4969-80 e15.
1180 58. Hartnell A, Steel J, Turley H, Jones M, Jackson DG, and Crocker PR.
1181 Characterization of human sialoadhesin, a sialic acid binding receptor expressed
1182 by resident and inflammatory macrophage populations. *Blood.* 2001;97(1):288-
1183 96.
1184 59. Vinson M, van der Merwe PA, Kelm S, May A, Jones EY, and Crocker PR.
1185 Characterization of the sialic acid-binding site in sialoadhesin by site-directed
1186 mutagenesis. *J Biol Chem.* 1996;271(16):9267-72.
1187 60. Huang J, Hume AJ, Abo KM, Werder RB, Villacorta-Martin C, Alysandratos KD, et
1188 al. SARS-CoV-2 Infection of Pluripotent Stem Cell-Derived Human Lung Alveolar
1189 Type 2 Cells Elicits a Rapid Epithelial-Intrinsic Inflammatory Response. *Cell Stem*
1190 *Cell.* 2020;27(6):962-73 e7.
1191 61. Son KN, Liang Z, and Lipton HL. Double-Stranded RNA Is Detected by
1192 Immunofluorescence Analysis in RNA and DNA Virus Infections, Including Those
1193 by Negative-Stranded RNA Viruses. *J Virol.* 2015;89(18):9383-92.

1194 62. Raj A, van den Bogaard P, Rifkin SA, van Oudenaarden A, and Tyagi S. Imaging
1195 individual mRNA molecules using multiple singly labeled probes. *Nat Methods.*
1196 2008;5(10):877-9.
1197 63. Scherer KM, Mascheroni L, Carnell GW, Wunderlich LCS, Makarchuk S,
1198 Brockhoff M, et al. SARS-CoV-2 nucleocapsid protein adheres to replication
1199 organelles before viral assembly at the Golgi/ERGIC and lysosome-mediated
1200 egress. *Sci Adv.* 2022;8(1):eabl4895.
1201 64. V'Kovski P, Kratzel A, Steiner S, Stalder H, and Thiel V. Coronavirus biology and
1202 replication: implications for SARS-CoV-2. *Nat Rev Microbiol.* 2021;19(3):155-70.
1203 65. Blanco-Melo D, Nilsson-Payant BE, Liu WC, Uhl S, Hoagland D, Moller R, et al.
1204 Imbalanced Host Response to SARS-CoV-2 Drives Development of COVID-19.
1205 *Cell.* 2020;181(5):1036-45 e9.
1206 66. Khan S, Shafiei MS, Longoria C, Schoggins JW, Savani RC, and Zaki H. SARS-
1207 CoV-2 spike protein induces inflammation via TLR2-dependent activation of the
1208 NF-kappaB pathway. *Elife.* 2021;10.
1209 67. Jensen S, and Thomsen AR. Sensing of RNA viruses: a review of innate immune
1210 receptors involved in recognizing RNA virus invasion. *J Virol.* 2012;86(6):2900-
1211 10.
1212 68. Kim YM, and Shin EC. Type I and III interferon responses in SARS-CoV-2
1213 infection. *Exp Mol Med.* 2021;53(5):750-60.
1214 69. Ablasser A, and Hur S. Regulation of cGAS- and RLR-mediated immunity to
1215 nucleic acids. *Nat Immunol.* 2020;21(1):17-29.
1216 70. Liu G, and Gack MU. Distinct and Orchestrated Functions of RNA Sensors in
1217 Innate Immunity. *Immunity.* 2020;53(1):26-42.
1218 71. Neufeldt CJ, Cerikan B, Cortese M, Frankish J, Lee JY, Plociennikowska A, et al.
1219 SARS-CoV-2 infection induces a pro-inflammatory cytokine response through
1220 cGAS-STING and NF-kappaB. *Commun Biol.* 2022;5(1):45.
1221 72. Di Domizio J, Gulen MF, Saidoune F, Thacker VV, Yatim A, Sharma K, et al. The
1222 cGAS-STING pathway drives type I IFN immunopathology in COVID-19. *Nature.*
1223 2022.
1224 73. Brinkmann MM, Spooner E, Hoebe K, Beutler B, Ploegh HL, and Kim YM. The
1225 interaction between the ER membrane protein UNC93B and TLR3, 7, and 9 is
1226 crucial for TLR signaling. *J Cell Biol.* 2007;177(2):265-75.
1227 74. Amraei R, Yin W, Napoleon MA, Suder EL, Berrigan J, Zhao Q, et al. CD209L/L-
1228 SIGN and CD209/DC-SIGN Act as Receptors for SARS-CoV-2. *ACS Cent Sci.*
1229 2021;7(7):1156-65.
1230 75. Wu Y, Wang F, Shen C, Peng W, Li D, Zhao C, et al. A noncompeting pair of
1231 human neutralizing antibodies block COVID-19 virus binding to its receptor
1232 ACE2. *Science.* 2020;368(6496):1274-8.
1233 76. Cao Y, Su B, Guo X, Sun W, Deng Y, Bao L, et al. Potent Neutralizing Antibodies
1234 against SARS-CoV-2 Identified by High-Throughput Single-Cell Sequencing of
1235 Convalescent Patients' B Cells. *Cell.* 2020;182(1):73-84 e16.
1236 77. Brouwer PJM, Caniels TG, van der Straten K, Snitselaar JL, Aldon Y, Bangaru S,
1237 et al. Potent neutralizing antibodies from COVID-19 patients define multiple
1238 targets of vulnerability. *Science.* 2020;369(6504):643-50.
1239 78. Suryadevara N, Shrihari S, Gilchuk P, VanBlargan LA, Binshtein E, Zost SJ, et al.
1240 Neutralizing and protective human monoclonal antibodies recognizing the N-

1241 terminal domain of the SARS-CoV-2 spike protein. *Cell.* 2021;184(9):2316-31
1242 e15.
1243 79. Klein S, Cortese M, Winter SL, Wachsmuth-Melm M, Neufeldt CJ, Cerikan B, et
1244 al. SARS-CoV-2 structure and replication characterized by in situ cryo-electron
1245 tomography. *Nat Commun.* 2020;11(1):5885.
1246 80. Thorne LG, Bouhaddou M, Reuschl AK, Zuliani-Alvarez L, Polacco B, Pelin A, et
1247 al. Evolution of enhanced innate immune evasion by SARS-CoV-2. *Nature.* 2021.
1248 81. Thorne LG, Reuschl AK, Zuliani-Alvarez L, Whelan MVX, Turner J, Noursadeghi
1249 M, et al. SARS-CoV-2 sensing by RIG-I and MDA5 links epithelial infection to
1250 macrophage inflammation. *EMBO J.* 2021;40(15):e107826.
1251 82. Yin X, Riva L, Pu Y, Martin-Sancho L, Kanamune J, Yamamoto Y, et al. MDA5
1252 Governs the Innate Immune Response to SARS-CoV-2 in Lung Epithelial Cells.
1253 *Cell Rep.* 2021;34(2):108628.
1254 83. Rebendenne A, Valadao ALC, Tauziet M, Maarifi G, Bonaventure B, McKellar J,
1255 et al. SARS-CoV-2 triggers an MDA-5-dependent interferon response which is
1256 unable to control replication in lung epithelial cells. *J Virol.* 2021.
1257 84. Sampaio NG, Chauveau L, Hertzog J, Bridgeman A, Fowler G, Moonen JP, et al.
1258 The RNA sensor MDA5 detects SARS-CoV-2 infection. *Sci Rep.*
1259 2021;11(1):13638.
1260 85. Dixit E, Boulant S, Zhang Y, Lee AS, Odendall C, Shum B, et al. Peroxisomes are
1261 signaling platforms for antiviral innate immunity. *Cell.* 2010;141(4):668-81.
1262 86. Esser-Nobis K, Hatfield LD, and Gale M, Jr. Spatiotemporal dynamics of innate
1263 immune signaling via RIG-I-like receptors. *Proc Natl Acad Sci U S A.*
1264 2020;117(27):15778-88.
1265 87. Horner SM, Liu HM, Park HS, Briley J, and Gale M, Jr. Mitochondrial-associated
1266 endoplasmic reticulum membranes (MAM) form innate immune synapses and are
1267 targeted by hepatitis C virus. *Proc Natl Acad Sci U S A.* 2011;108(35):14590-5.
1268 88. Ural BB, Yeung ST, Damani-Yokota P, Devlin JC, de Vries M, Vera-Licona P, et
1269 al. Identification of a nerve-associated, lung-resident interstitial macrophage
1270 subset with distinct localization and immunoregulatory properties. *Sci Immunol.*
1271 2020;5(45).
1272 89. Akiyama H, and Gummuluru S. HIV-1 Persistence and Chronic Induction of
1273 Innate Immune Responses in Macrophages. *Viruses.* 2020;12(7).
1274 90. Park A, and Iwasaki A. Type I and Type III Interferons - Induction, Signaling,
1275 Evasion, and Application to Combat COVID-19. *Cell Host Microbe.*
1276 2020;27(6):870-8.
1277 91. Sa Ribero M, Jouvenet N, Dreux M, and Nisole S. Interplay between SARS-CoV-
1278 2 and the type I interferon response. *PLoS Pathog.* 2020;16(7):e1008737.
1279 92. Sodeifian F, Nikfarjam M, Kian N, Mohamed K, and Rezaei N. The role of type I
1280 interferon in the treatment of COVID-19. *J Med Virol.* 2022;94(1):63-81.
1281 93. Klouda T, Hao Y, Kim H, Kim J, Olejnik J, Hume AJ, et al. Interferon-alpha or -
1282 beta facilitates SARS-CoV-2 pulmonary vascular infection by inducing ACE2.
1283 *Angiogenesis.* 2021.
1284 94. Beigel JH, Tomashek KM, Dodd LE, Mehta AK, Zingman BS, Kalil AC, et al.
1285 Remdesivir for the Treatment of Covid-19 - Final Report. *N Engl J Med.*
1286 2020;383(19):1813-26.
1287 95. Kalligeros M, Tashima KT, Mylona EK, Rybak N, Flanigan TP, Farmakiotis D, et
1288 al. Remdesivir Use Compared With Supportive Care in Hospitalized Patients With

1289 Severe COVID-19: A Single-Center Experience. *Open Forum Infect Dis.*
1290 2020;7(10):ofaa319.
1291 96. Kalil AC, Patterson TF, Mehta AK, Tomashek KM, Wolfe CR, Ghazaryan V, et al.
1292 Baricitinib plus Remdesivir for Hospitalized Adults with Covid-19. *N Engl J Med.*
1293 2021;384(9):795-807.
1294 97. Miller CM, Akiyama H, Agosto LM, Emery A, Ettinger CR, Swamstrom RI, et al.
1295 Virion associated Vpr alleviates a post-integration block to HIV-1 infection of
1296 dendritic cells. *Journal of virology.* 2017.
1297 98. Hatch SC, Archer J, and Gummuluru S. Glycosphingolipid composition of human
1298 immunodeficiency virus type 1 (HIV-1) particles is a crucial determinant for
1299 dendritic cell-mediated HIV-1 trans-infection. *J Virol.* 2009;83(8):3496-506.
1300 99. Thi Nhu Thao T, Labroussaa F, Ebert N, V'Kovski P, Stalder H, Portmann J, et al.
1301 Rapid reconstruction of SARS-CoV-2 using a synthetic genomics platform.
1302 *Nature.* 2020;582(7813):561-5.
1303 100. Liao M, Wu J, Dai M, Li H, Yan N, Yuan R, et al. Rapid detection of SARS-CoV-2,
1304 replicating or non-replicating, using RT-PCR. *Int J Infect Dis.* 2021;104:471-3.
1305 101. Livak KJ, and Schmittgen TD. Analysis of relative gene expression data using
1306 real-time quantitative PCR and the 2(-Delta Delta C(T)) Method. *Methods.*
1307 2001;25(4):402-8.
1308

Figure 1

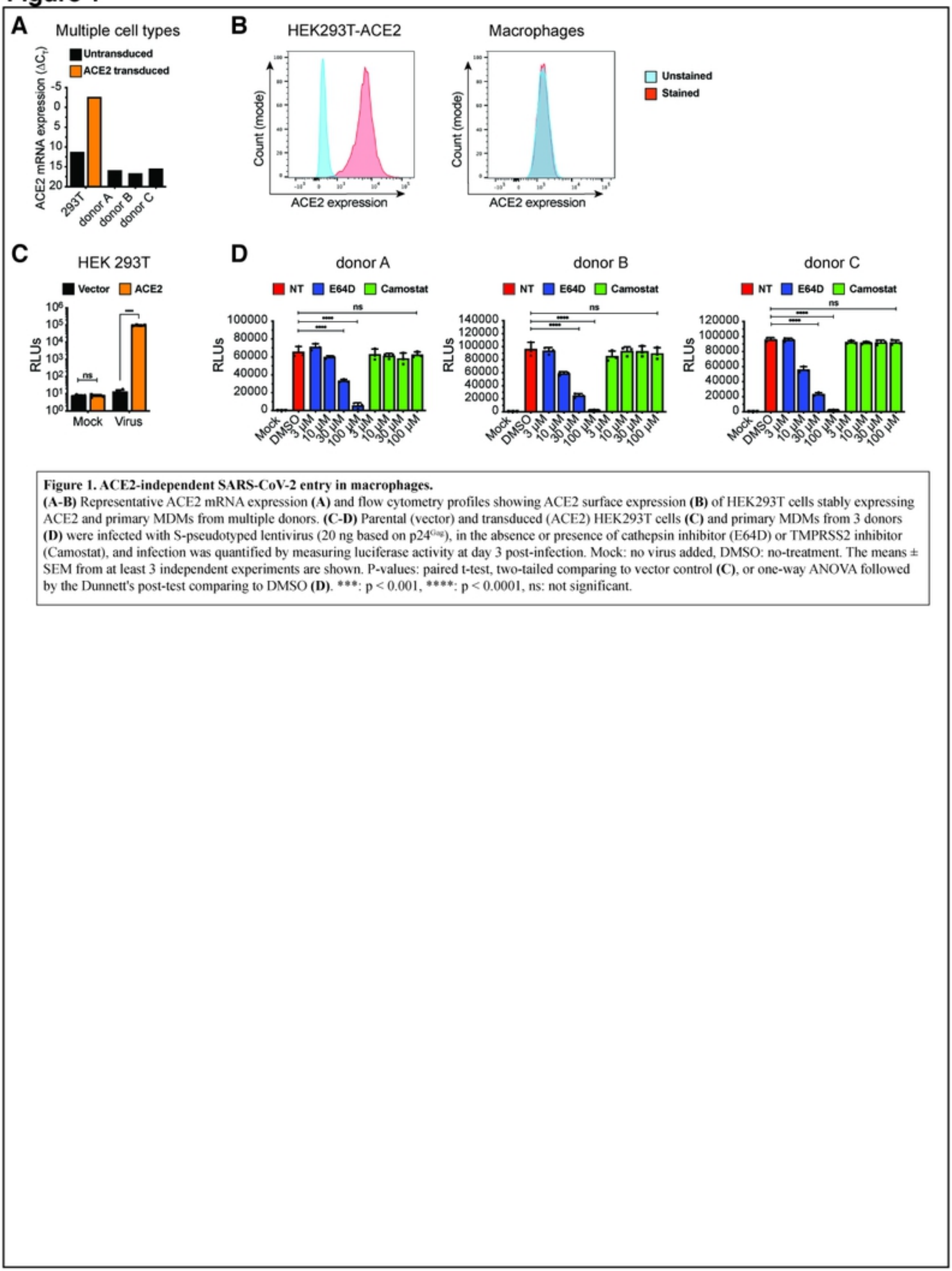

Figure 1. ACE2-independent SARS-CoV-2 entry in macrophages.
(A-B) Representative ACE2 mRNA expression **(A)** and flow cytometry profiles showing ACE2 surface expression **(B)** of HEK293T cells stably expressing ACE2 and primary MDMs from multiple donors. **(C-D)** Parental (vector) and transduced (ACE2) HEK293T cells **(C)** and primary MDMs from 3 donors **(D)** were infected with S-pseudotyped lentivirus (20 ng based on $p24^{Gag}$), in the absence or presence of cathepsin inhibitor (E64D) or TMPRSS2 inhibitor (Camostat), and infection was quantified by measuring luciferase activity at day 3 post-infection. Mock: no virus added, DMSO: no-treatment. The means ± SEM from at least 3 independent experiments are shown. P-values: paired t-test, two-tailed comparing to vector control **(C)**, or one-way ANOVA followed by the Dunnett's post-test comparing to DMSO **(D)**. ***: $p < 0.001$, ****: $p < 0.0001$, ns: not significant.

Figure 1

Figure 2

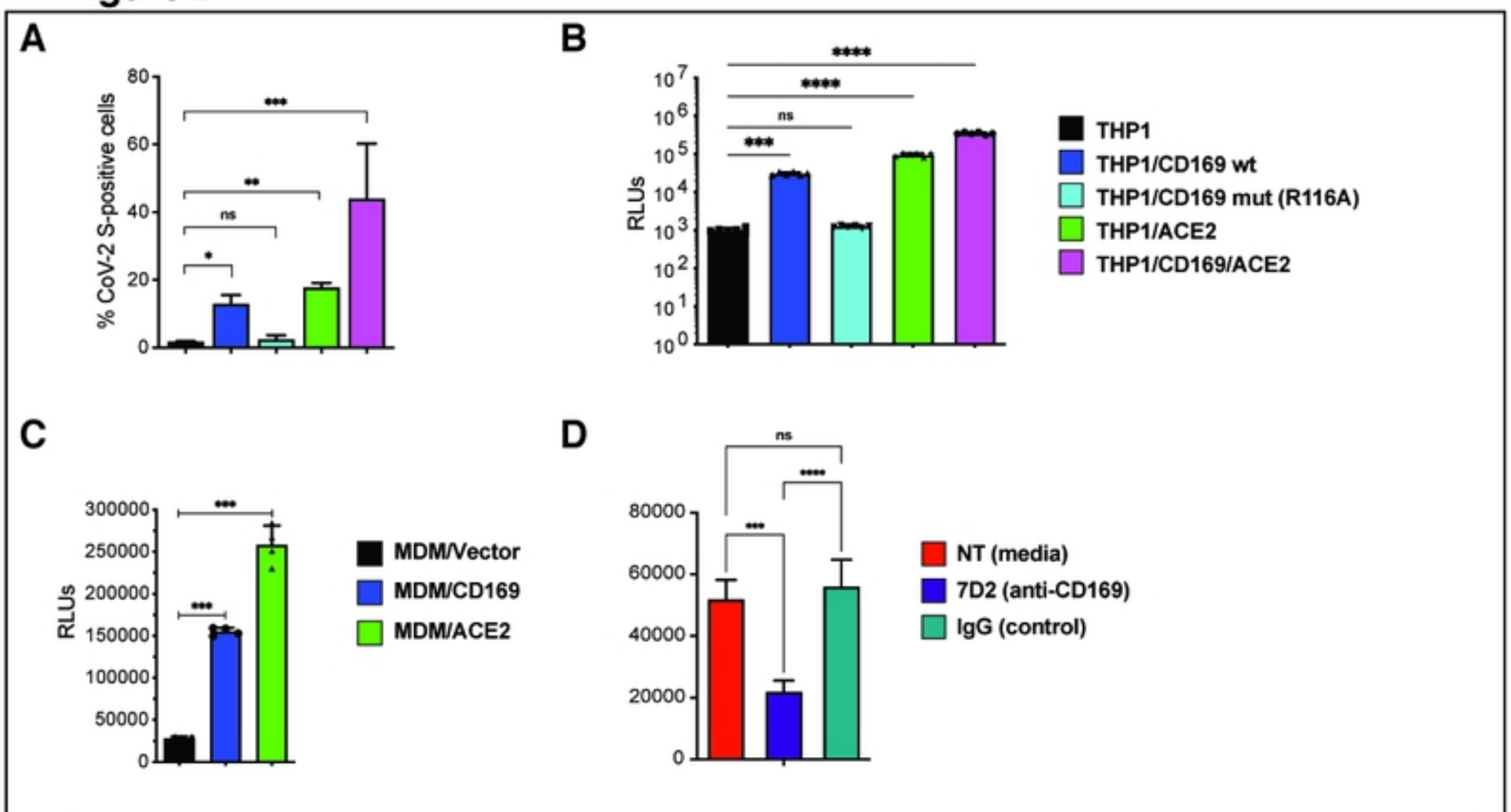

Figure 2. CD169 is a SARS-CoV-2 attachment and entry factor in macrophages.
(A) Binding of SARS-CoV-2 S protein (Wuhan isolate) to THP1 monocytes expressing wt CD169, mutant CD169 (R116A), ACE2, or both wt CD169 and ACE2 (CD169/ACE2). **(B)** THP1/PMA macrophages were infected with S-pseudotyped lentivirus (20 ng $p24^{Gag}$), and infection was quantified by measuring luciferase activity at 3 dpi. Relative light units (RLUs) from each cell line were normalized to no virus control (mock). The means ± SEM are shown from at least five independent experiments. **(C)** Primary MDMs from three donors overexpressing either CD169 or ACE2, or control were infected with S-pseudotyped lentivirus (20 ng $p24^{Gag}$) for 3 days, followed by analysis of luciferase activity in whole cell lysates. **(D)** Untransduced primary MDMs (representative of 3 donors) were pre-treated with anti-CD169 mAb (20 µg/ml, 7D2), IgG1, or empty media for 30 minutes at 4°C prior to infection with S-pseudotyped lentivirus (20 ng $p24^{Gag}$) for 3 days, followed by analysis of luciferase activity. RLUs from each donor in each group were normalized to no virus control (mock). The means ± SEM from at least 3 independent experiments are shown. P-values: paired t-test, two-tailed **(A)**, one-way ANOVA followed by the Dunnett's post-test **(B)** or Tukey's post-test comparing to parental (THP1) cells **(C)** or each pre-treatment condition **(D)**. ***: $p < 0.001$, ****: $p < 0.0001$, ns: not significant.

Figure 2

Figure 3

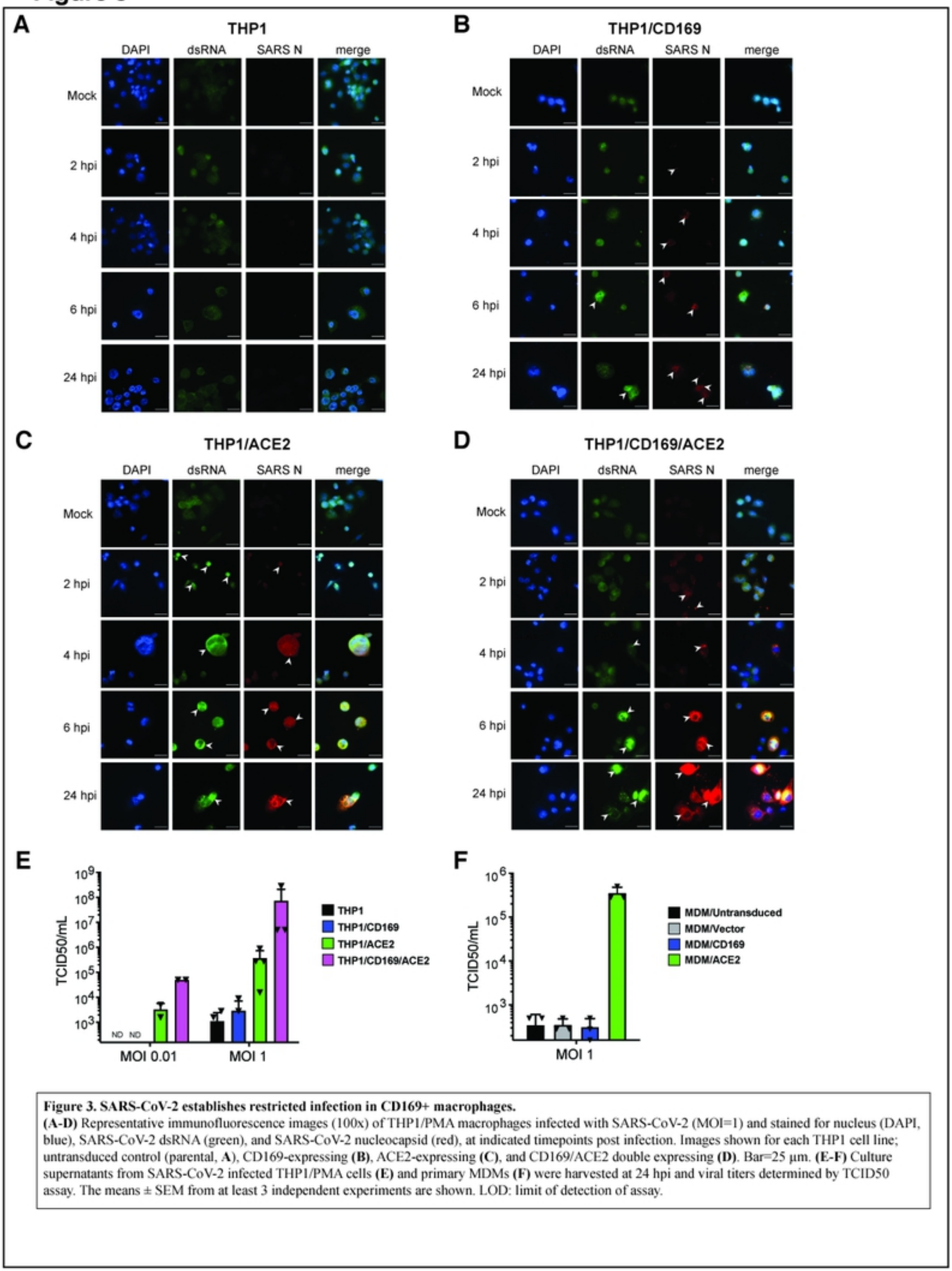

Figure 3. SARS-CoV-2 establishes restricted infection in CD169+ macrophages.
(A-D) Representative immunofluorescence images (100x) of THP1/PMA macrophages infected with SARS-CoV-2 (MOI=1) and stained for nucleus (DAPI, blue), SARS-CoV-2 dsRNA (green), and SARS-CoV-2 nucleocapsid (red), at indicated timepoints post infection. Images shown for each THP1 cell line; untransduced control (parental, **A**), CD169-expressing **(B)**, ACE2-expressing **(C)**, and CD169/ACE2 double expressing **(D)**. Bar=25 µm. **(E-F)** Culture supernatants from SARS-CoV-2 infected THP1/PMA cells **(E)** and primary MDMs **(F)** were harvested at 24 hpi and viral titers determined by TCID50 assay. The means ± SEM from at least 3 independent experiments are shown. LOD: limit of detection of assay.

Figure 3

Figure 4

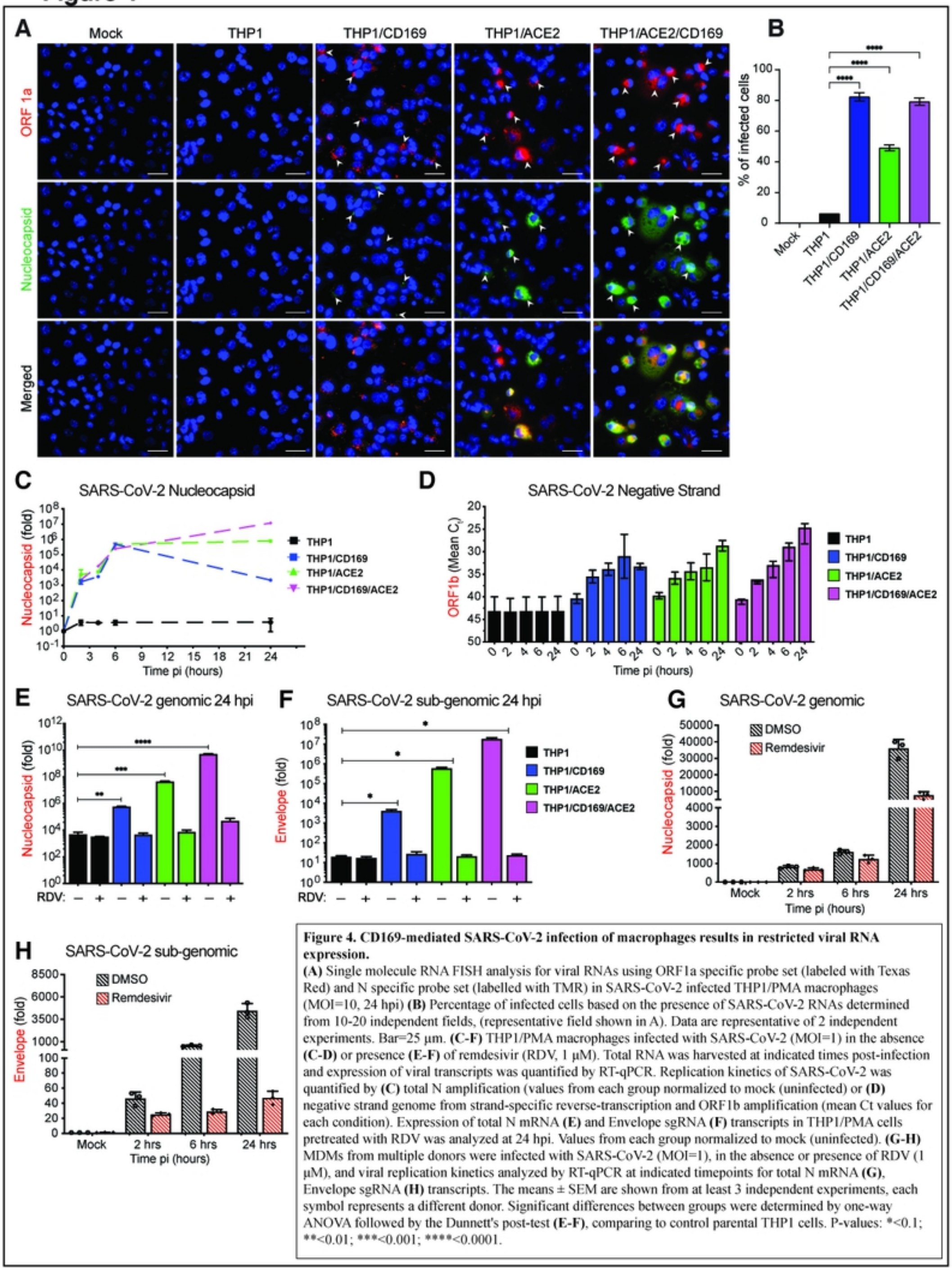

Figure 4. CD169-mediated SARS-CoV-2 infection of macrophages results in restricted viral RNA expression.
(A) Single molecule RNA FISH analysis for viral RNAs using ORF1a specific probe set (labeled with Texas Red) and N specific probe set (labelled with TMR) in SARS-CoV-2 infected THP1/PMA macrophages (MOI=10, 24 hpi) **(B)** Percentage of infected cells based on the presence of SARS-CoV-2 RNAs determined from 10-20 independent fields, (representative field shown in A). Data are representative of 2 independent experiments. Bar=25 µm. **(C-F)** THP1/PMA macrophages infected with SARS-CoV-2 (MOI=1) in the absence **(C-D)** or presence **(E-F)** of remdesivir (RDV, 1 µM). Total RNA was harvested at indicated times post-infection and expression of viral transcripts was quantified by RT-qPCR. Replication kinetics of SARS-CoV-2 was quantified by **(C)** total N amplification (values from each group normalized to mock (uninfected) or **(D)** negative strand genome from strand-specific reverse-transcription and ORF1b amplification (mean Ct values for each condition). Expression of total N mRNA **(E)** and Envelope sgRNA **(F)** transcripts in THP1/PMA cells pretreated with RDV was analyzed at 24 hpi. Values from each group normalized to mock (uninfected). **(G-H)** MDMs from multiple donors were infected with SARS-CoV-2 (MOI=1), in the absence or presence of RDV (1 µM), and viral replication kinetics analyzed by RT-qPCR at indicated timepoints for total N mRNA **(G)**, Envelope sgRNA **(H)** transcripts. The means ± SEM are shown from at least 3 independent experiments, each symbol represents a different donor. Significant differences between groups were determined by one-way ANOVA followed by the Dunnett's post-test **(E-F)**, comparing to control parental THP1 cells. P-values: *<0.1; **<0.01; ***<0.001; ****<0.0001.

Figure 4

Figure 5

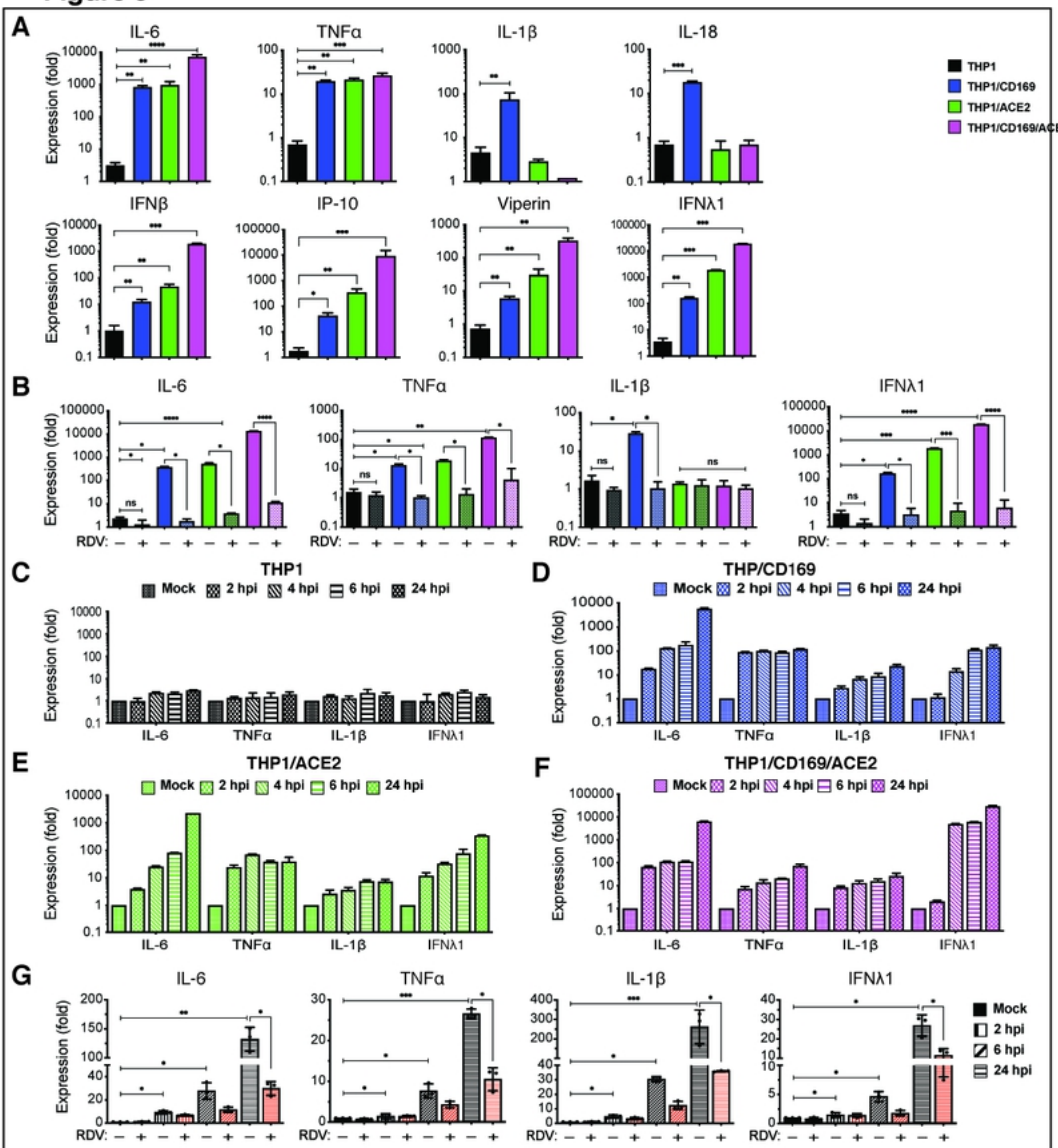

Figure 5. Restricted expression of SARS-CoV-2 gRNA and sgRNA induces pro-inflammatory responses in non-productively infected macrophages
(A-B) PMA-differentiated THP1 cells from parental (THP1) or those expressing CD169, ACE2, or CD169/ACE2 were infected with SARS-CoV-2 (MOI=1, 24 hpi) in the absence or presence of RDV (1 µM, 30 mins), and total RNA was quantified by RT-qPCR for pro-inflammatory cytokines and ISGs. Values were normalized to mock-infected control for each group. Fold-induction for indicated pro-inflammatory cytokines (**A**, **top panel**) and ISGs (**A**, **bottom panel**) in the absence of RDV, or in the presence of RDV **(B)**. **(C-F)** Kinetics of pro-inflammatory cytokine/ISG mRNA expression in the absence of RDV in parental **(C)**, CD169-expressing **(D)**, ACE2-expressing **(E)**, and CD169/ACE2-expressing **(F)** PMA-differentiated THP1 cells. **(G)** MDMs from multiple donors were infected with SARS-CoV-2 (MOI=1, 24 hpi) and total RNA analyzed by RT-qPCR. MDMs were pre-treated with DMSO (control) or RDV (1 µM, 30 mins) prior to infection, and fold-induction of indicated cytokine mRNAs normalized to mock-infected controls from each donor. RDV: Remdesivir, ISGs: interferon-stimulated genes. Minus sign represents DMSO, and plus sign represents RDV pre-treatment. The means ± SEM from at least 3 independent experiments are shown. Significant differences between groups were determined by one-way ANOVA followed by the Dunnett's post-test between groups **(A)** or Tukey's multiple comparisons test within groups (**B** and **G**), comparing to parental THP1 **(A)** or DMSO-treated (**B**, **G**) in each group. P-values: *<0.1; **<0.01; ***<0.001; ****<0.0001, ns: not significant.

Figure 5

Figure 6

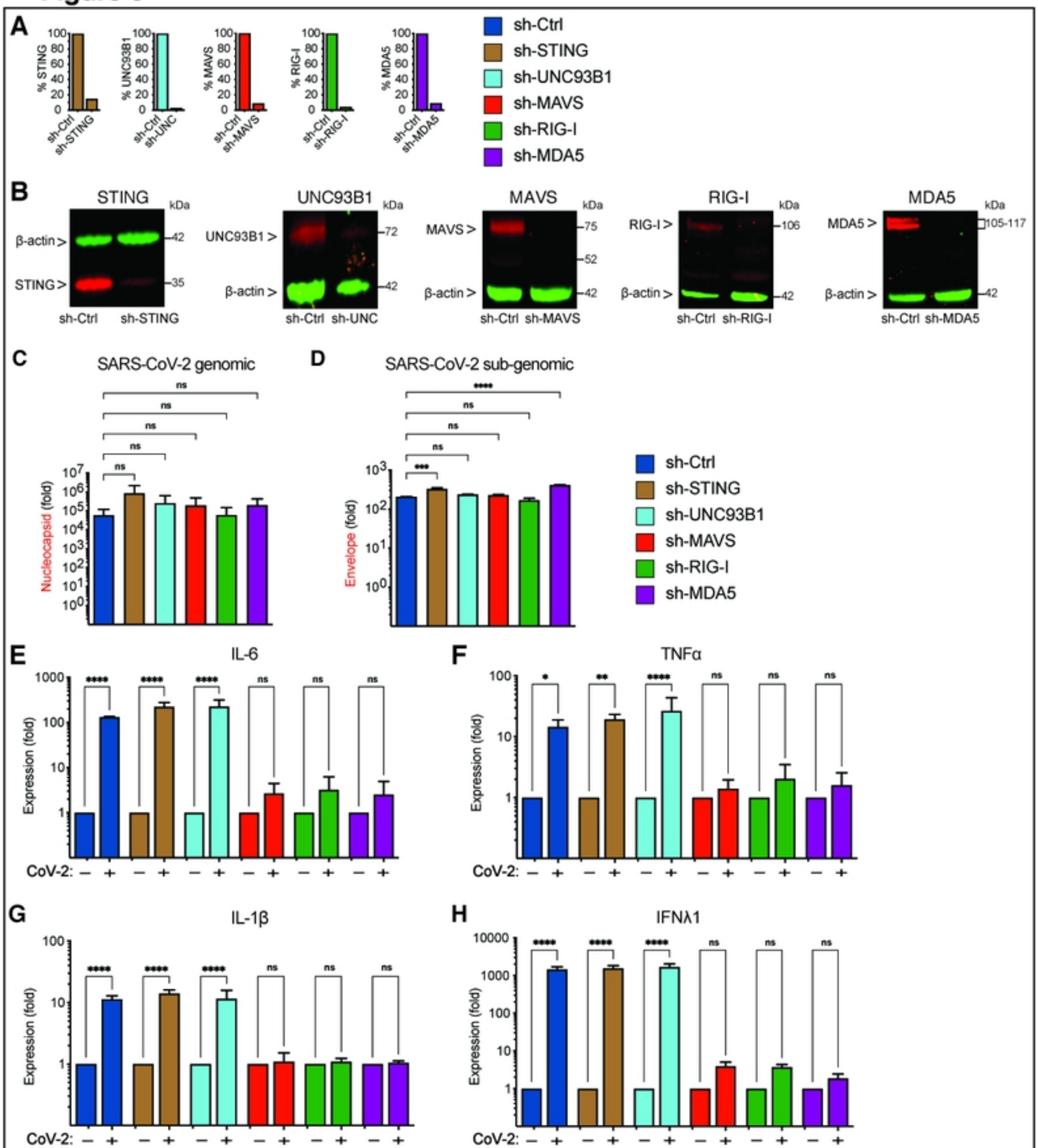

Figure 6. Cytosolic RNA sensing by RIG-I and MDA-5 is required for SARS-CoV-2 induced innate immune responses in macrophages
(A-B) CD169-expressing THP1 monocytes were transduced with lentivectors expressing shRNA against non-specific control (scramble), or specific sequences against STING, UNC93B1, MAVS, RIG-I, and MDA-5. Knockdown of host proteins targeted by shRNAs compared to scramble analyzed by RT-qPCR **(A)**, and immune blotting **(B)**. (C-H) CD169+ THP1 cells with stable knockdown of target genes were PMA-differentiated and infected with SARS-CoV-2 (MOI=1, 24 hpi), and total RNA was analyzed by RT-qPCR for total nucleocapsid (gRNA) **(C)**, sgRNA (Envelope) **(D)**, and pro-inflammatory cytokines/ISGs, IL6, TNFα, IL-1β and IFNλ1 **(E-F)**, normalized to mock-infected controls for each group. Each knockdown is represented by different colors as in A. The means ± SEM from 3 independent experiments are shown, and significant differences were determined by one-way ANOVA followed by the Dunnett's post-test comparing to scramble THP1 **(C-D)**, or two-way ANOVA followed by Bonferroni post-test comparing Mock to CoV-2+ in each group **(E-H)**. P-values: *<0.1; **<0.01; ***<0.001; ****<0.0001), ns: not significant.

Figure 6

Figure 7

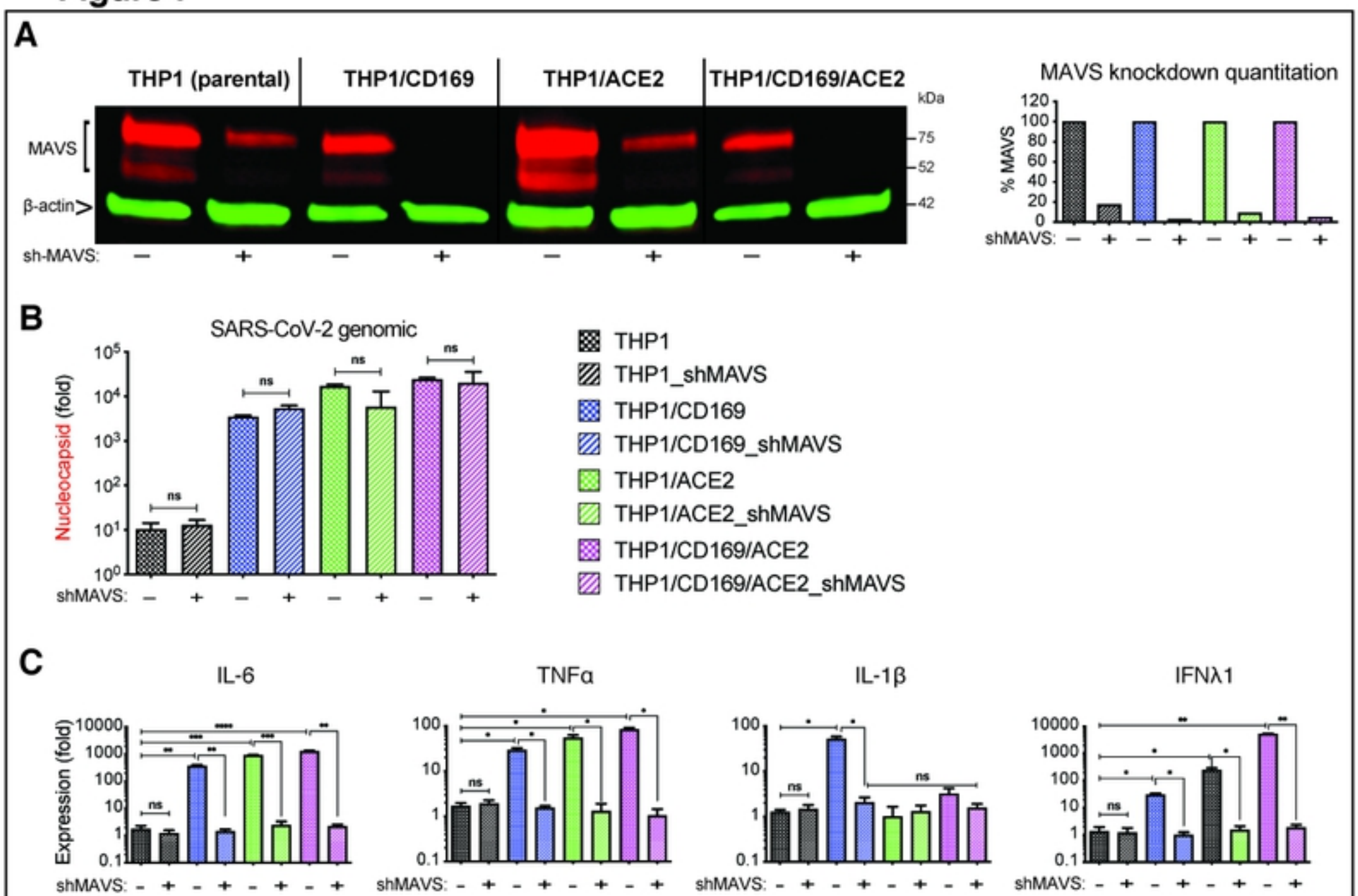

Figure 7. MAVS is essential for SARS-CoV-2 RNA-induced inflammatory responses in macrophages.
(A) Parental (THP1) monocytes and those expressing CD169, ACE2, or CD169/ACE2 were transduced with lentivectors expressing shRNA against scrambled sequence (-), or MAVS sequence (+), and knockdown of MAVS in each cell line analyzed by immune blotting (A, left panel), and quantified (**A, right panel**). **(B-C)** THP1 monocytes with stable MAVS knockdown were PMA-differentiated and infected with SARS-CoV-2 (MOI=1, 24 hpi), and total RNA analyzed by RT-qPCR for **(B)** total viral transcripts (nucleocapsid), and **(C)** IL6, TNFα, IL-1β and IFNλ1 mRNA expression, normalized to mock-infected controls for each group. The means ± SEM from 3 independent experiments are shown, and significant differences were determined by one-way ANOVA followed by the Tukey-Kramer post-test within groups (**B**, and **C**), or Dunnett's post-test between groups **(C)**. P-values: *<0.05; **<0.01; ***<0.001; ****<0.0001, ns: not significant.

Figure 7